EXCITATION OF THE IONIZED NITROGEN MOLECULE IN THE AURORA

By

Kim Nielsen

RECOMMENDED:

Advisory Committee Chair

Department Head

APPROVED:

Dean, College of Science, Engineering and Mathematics

Dean of Graduate School

1-6-03

Date

EXCITATION OF THE IONIZED NITROGEN MOLECULE IN THE AURORA

A

THESIS

Presented to the Faculty

of the University of Alaska Fairbanks

in Partial Fulfillment of the Requirements

for the Degree of

MASTER OF SCIENCE

By

Kim Nielsen, B.S.

Fairbanks, Alaska

December 2002

Abstract

An understanding of the excitation mechanism of the ionospheric molecules during auroral activity is of vital importance for the overall ionospheric understanding including its interaction with the magnetosphere. In this thesis we study two emissions originating from the excited nitrogen molecule ion. The first negative (0,1) emission at 4278 Å originating from the B state, and Meinel (2,0) emission at 7852 Å originating from the A state during moderate to strong aurora have been observed with an imaging spectrograph at Poker Flat, Alaska. The B state has a short lifetime compared to the inverse collision frequency at auroral altitudes, while the A state can be deactivated during collisions at altitudes near 95 km. The B state can be populated by an up-welling of N_2^+ into sunlit regions. Both processes are expected to depend on auroral activity. If none of the processes are present we expect a constant ratio between the two emissions. Data for three nights have been studied and a constant ratio was found at all times. Thus neither deactivation of the A state or up-welling of the ion seem to appear during the observations presented here. The values of the ratio for the three nights are 2.53 ± 0.38, 3.05 ± 0.22, and 3.40 ± 1.10, respectively.

Contents

List of Figures vi
List of Tables ix
Acknowledgements x

1 Introduction **1**

2 Excitation and Emission of N_2^+ **4**
2.1 Formation of the N_2^+ Molecule 4
2.1.1 Particle Impact 6
2.1.2 Charge Transfer 12
2.1.3 Ion-atom Interchange 13
2.1.4 Dissociation 13
2.1.5 Quenching 14
2.1.6 Cascading 15
2.1.7 Resonance Scattering 16
2.2 Emission 16
2.3 Summary 18

3 Instrumentation **20**
3.1 The Imaging Spectrograph 20
3.2 Data Acquisition and Software 21

4 Processing of Data **26**
4.1 Calibration of Data 26
4.1.1 Calibration for Read-out Noise 29

4.1.2 Calibration for Dark Current 29
4.1.3 Calibration for CDD Defects 31
4.1.4 Calibration for Curvature Effect 31
4.1.5 Calibration for Vignetting Effects 32
4.1.6 Wavelength Calibration 33
4.1.7 Absolute (Intensity) Calibration 36
4.1.8 Atmospheric Corrections 38
4.2 Data Analysis 38
4.2.1 Calculating the Emission 40
4.2.2 Error Analysis 41

5 Results and Discussion **43**
5.1 Observations 43
5.2 Discussion 53

6 Conclusion **57**

Bibliography **59**

List of Figures

2.1 Potential curves for the N_2 and N_2^+ including some excited states. From *Rees* [1989]. 5

2.2 Excitation cross section data for total N_2^+, $N_2^+(A)$, and $N_2^+(B)$. From *Cartwright et al.* [1975]. The references listed in the plot are *Pendleton Jr. and Weaver* [1973]; *Borst and Zipf* [1970]; *Simpson and McConkey* [1969]; *Stanton and John* [1969]; *Srivastava and Mirza* [1968, 1969]; *Holland and Maier II* [1972, 1973]; *Shemansky and Broadfoot* [1971] 10

2.3 Altitude profile of the total Meinel/first negative ratio. The dashed line indicates the result without quenching of the A state. From *Cartwright et al.* [1975]. The references listed are *Harrison* [1969, 1972]; *Vallance Jones* [1971]; *Gattinger and Vallance Jones* [1972]; *Vaisberg* [1962]; *Gattinger* [1961]. . . . 15

2.4 Cross section curves for the N_2^+, and the lower lying excited states. The similar shapes for the A, B, and D states are clear. The different shape of the C state might be due to a different ionization process than the one involved for production of the A, B, and D states. From *Fons et al.* [1994]. The references listed are *Stanton and John* [1969] (ref.1), *Borst and Zipf* [1970] (ref.4), *van de Runstraat et al.* [1974] (ref. 9), and *Itakawa et al.* [1986] (ref.12). 18

3.1 Schematic block diagram of the experiment set-up. 22

3.2 Schematic of the imaging spectrograph. The detector is shown in next figure. Redrawn from *Semeter* [1997]. 23

3.3 Schematic of the detector used in the instrument. Redrawn from *Semeter* [1997]. 24

4.1 This image, showing the auroral spectra in the 7000 Å window, illustrates a typical raw data image. The wavelength is increasing from left to right with 7000 Å being near the center of the image. The vertical dimension is the spatial dimension. 27

4.2 The image shows a spectrum obtained with a standard lamp. The lamp emits at all wavelengths and the image should be uniform in the direction of the slit (vertical dimension in image). The plot shows a column profile from the center part of the image. The vignetting is shown as a slow drop in intensity towards the edges. The steep drops in intensity at the edges is not vignetting but merely shows the limit of the projected image, in other words, the projection does not fill the CCD's field. 28

4.3 The average dark current per pixel plus read-out noise as a function of integration time (in frames). The read-out noise is constant and are determined as the signal obtained with zero integration time. 30

4.4 The actual image for further analysis after being reduced to a narrower image, and thus neglecting curvature effects. The magnetic zenith is the center of the image in the wavelength direction. 32

4.5 An incoming beam of light incident on a diffraction grating. From *Gray* [1992]. 34

4.6 Two beams of light entering a camera. This figure is shown to help illustrate the constant linear dispersion. From *Gray* [1992]. 35

4.7 The emission curve from the standard lamp measured in Rayleigh as function of wavelength in Ångstrom. 37

4.8 A typical spectra from the 4200 and 7700 ranges showing the brightness as a function of wavelength. These spectra was obtained during relative strong auroral activity. The emissions relative close to the 4278 and 7852 emissions are also identified. 39

5.1 First plot showing the time series of Meinel (2,0) and first negative (0,1) emissions, March 19, 2001. Second plot shows the corresponding time series of the Meinel (2,0) and first negative (0,1) ratio. 45
5.2 First plot showing the time series of Meinel (2,0) and first negative (0,1) emissions, March 23, 2001. Second plot shows the corresponding time series of the Meinel (2,0) and first negative (0,1) ratio. 46
5.3 First plot showing the time series of Meinel (2,0) and first negative (0,1) emissions, March 31, 2001. Second plot shows the corresponding time series of the Meinel (2,0) and first negative (0,1) ratio. 47
5.4 Time series for auroral activity seen with the All-sky camera located at Poker Flat, March 19, 2001. The time scale shown is in UT time while the spatial scale ranges from north to south. 48
5.5 Scatter plot of the Meinel (2,0) and first negative (0,1), March 19, 2001. A linear regression line is superimposed upon the plot and the regression parameters shown. In addition, the correlation coefficient is given. 49
5.6 Time series for auroral activity seen with the All-sky camera located at Poker Flat, March 23, 2001. The time scale shown is in UT time while the spatial scale ranges from north to south. 50
5.7 Scatter plot of the Meinel (2,0) and first negative (0,1), March 23, 2001. A linear regression line is superimposed upon the plot and the regression parameters shown. In addition, the correlation coefficient is given. 51
5.8 Scatter plot of the Meinel (2,0) and first negative (0,1), March 19, 2001. A linear regression line is superimposed upon the plot and the regression parameters shown. In addition, the correlation coefficient is given. 52

List of Tables

2.1 Cross section data for the ground state of N_2^+ and the two excited states. . 9

4.1 The transmission coefficient for the first negative (0,1), first positive (3,1), and Meinel (2,0). 38

Acknowledgements

Your life depends on so many decisions and even the smallest spontaneous decisions can make a large impact on your future life. Had anyone asked me 5 years ago where I would be today I am sure the answer would had been Copenhagen, Denmark. But it didn't turned out that way and I am very grateful for the opportunity to come to UAF to work on my master thesis. Many people have helped me to get here and make my stay a wonderful experience, and I would like to thank them. First, to Hans C. Stenbaek-Nielsen, whom I came in contact with while I was in Denmark and later became my advisor. He have given me the opportunity to become involved in experimental aeronomy and given me insight to how research works. He have allowed me to work on my own pace and learning with him as an advisor has been tremendous. Much of this thesis have been developing programs to analyze the data. I could not have done this without the help from Dirk Lummerzheim. The rest of my committee, Roger Smith, and Brenton Watkins have in similar ways been patient and helped with valuable discussions.

The observations would have been difficult to perform without the crew at Poker Flat Research Range, Alaska. A special thought to June and Brian for keeping the science center running.

For the development of the software to operate the imaging spectrograph many words was sworn. Without the help from Ed Hoch I am sure it would not had gone far. Tom Hallinan and Jeffrey Baumgardner have been a invaluable help discussing problems associated with the instrument.

I would like to thanks my friends up here in Fairbanks, and especially John Chappelow who have helped me many times moving the instrument and proven a good physics discussion partner.

Irene Downes have been a great help with everything. From paper work to giving me a ride to work when my car couldn't start at 40 below. Not just me, but the most of all us graduate students in Physics at UAF wouldn't have made it without her.

Back home in Denmark I would like to show my appreciation to my friends who helped me out with my decision to attend UAF. A special gratitude to Helle who got me started and pushed me to go through with it. The Julie Damms Studidefond and Axel Wiin's

Rejselegat for making my travel and stay to Fairbanks possible.

Finally, my family for their unlimited support. Especially my parents and grand parents, of whom I lost three the last year. I wish I could have been done while you were still around. They have always believed in me and letting me choose my own ways. Thank you !

Chapter 1

Introduction

Observations of auroral phenomena dates back to the classical antiquity in Europe and ancient Asia [*Silverman*, 1998]. In polar regions where the aurora is quite common it was believed that the aurora was the home of dead souls or gods. The specific myths are just as many as the there are villages in those regions. Further south, where aurora is rare, it was surrounded by fear and believed to messages from god or portens of coming events. Thus, aurora was associated with wars and epidemic disasters like the great plague.

Recordings of the early observations of the aurora can be found [*Silverman*, 1998] from the classical Greece and Rome, e.g. Aristotle, Livy's history of Rome, from the Middle East in the Bible, and finally, Asian annals. The aurora also caught the attention of early scientists like Galileo, who named it Aurora Borealis after the goddess of dawn and Descartes, who thought of it as a powerful terrestrial flame reflected of the clouds. Other well-known scientists like Halley, Tycho Brahe, M. V. Lomonosov, Ångström, Celcius, and Cavendish also showed interest in solving the mysterious aurora [e.g. *Silverman*, 1998; *Christensen et al.*, 1998; *Brekke and Egeland*, 1994; *Vallance Jones*, 1974].

With the beginning of our classical picture of our world in the seventeenth century several scientists tried to explain the aurora. Galileo, for example, thought of the aurora as a reflection of sunlight in the air[1]. The invention of the telescope made it possible to study sunspots and a connection between solar activity and auroral activity was found. Together with the exploration of the geomagnetic field in the early nineteenth century the pioneering work in auroral physics was founded.

[1] http://www.gi.alaska.edu/ScienceForum/SF3/368.html

The modern understanding of the aurora starts with Kristian Birkeland. Together with earlier observations and the knowledge in electromagnetism at that time he was able to conduct his famous terella experiment. The theoretical understanding of the emission in the aurora, however, first came with the development of the classical quantum mechanics. During that time the development of spectroscopy took off and scientists were now able through laboratory experiments to identify the source molecule for an emission. It took some time, however, to identify some of the auroral emissions due to that some of the emissions originate from metastable states. This was (and still is) an experimental problem in laboratories when the collision frequency is comparable to the inverse lifetime of the mestable state. Thus, the metastable state can be de-activated by collisions before radiating. At auroral altitude the collision frequency is low enough for some metastable states to decay by radiation.

Our upper atmosphere consist mainly of O_2, N_2, and atomic oxygen. The energetic particles that penetrate down to the atmosphere lose their energy through collisions with the atmospheric constituents. The energy is then deposited into excitation, ionization, or dissociation of the atmospheric atoms and molecules, producing various atoms and ions from the main constituents, like the ionized nitrogen molecule. The auroral spectrum consists of emissions in all the possible transitions that can occur between states of the resulting particles.

Description of the N_2^+ molecule requires fundamentals in atomic and molecular physics. The purpose of this thesis is to describe the excitation of this molecule in a very specific environment, the earth's ionosphere, to be more specific, excitation in the aurora.

Ionization and excitation of the nitrogen molecule in the aurora is created primarily by the processes

- Particle impact
- Photon absorption
- Chemical reactions

These processes and their importance for excitation of N_2^+ will be discussed in more depth in the following chapters.

From optical spectra of the aurora several physical features can be extracted. Our interest is connected to the processes involving the production of the $N_2^+(A)$ and $N_2^+(B)$ states. These two states are the origin of the prominent emissions of the first negative (1N) band, $N_2^+(B) \rightarrow N_2^+(X)$, and the Meinel (M) band $N_2^+(A) \rightarrow N_2^+(X)$, where A, and B are the two excited states while X is the ground state. The main source for excitation to these two states in the aurora are collisions with incoming energetic electrons [e.g. *Gattinger and Vallance Jones*, 1972; *Vallance Jones*, 1974; *Rees*, 1989]. Laboratory experiments have shown that the direct excitation cross-section for electron impact on N_2 creating the two states are strictly proportional [*Simpson and McConkey*, 1969]. If the only excitation process is electron impact, then we can interpret the emission cross sections as excitation cross sections [*Simpson and McConkey*, 1969; *Cartwright et al.*, 1975]. This implies that we would expect the emission ratio of the two bands to be constant. In fact, *Piper et al.* [1986] showed a constant value for individual bands independent of electron beam energies. However, *Gattinger and Vallance Jones* [1972] postulated a decrease in the first negative to Meinel intensity ratio with auroral brightness. This is in contrast to the experiment by *Cartwright et al.* [1975], who found a constant ratio above the quenching height of Meinel emission (≈ 120 km). Also, *Remick et al.* [2001] found that the $1N(0,1)$ brightness increased above the proportionality rate during strong auroral activity in contrast to the postulate by *Gattinger and Vallance Jones* [1972]. Despite many years of auroral research it is surprising that we still have not solved this problem. For the first case, a decrease in the $\frac{1N}{M}$ ratio, it has been suggested [*Omholt*, 1957], that it might be due to the charge transfer process

$$O^+(^2D;^2P) + N_2(X^3\Sigma) \rightarrow O(^3P) + N_2^+(A^2\Pi). \tag{1.1}$$

This process will enhance the $N_2^+(A)$ population and thus increase the observed integrated intensity. Finally, a larger ratio has been attributed to an upwelling of $N_2^+(X)$ into sunlit regions, increasing the $N_2^+(B)$ population by resonant scattering [*Remick et al.*, 2001].

I here present data obtained from Poker Flat, Alaska, during a two week span in March 2001. Using an imaging spectrograph orientated towards magnetic zenith, observations of the auroral spectra have been made. The N_2^+ first negative $(0,1)$ (4278 Å) and the N_2^+ Meinel $(2,0)$ (7852 Å) are being used to test the proportionality between the two bands.

Chapter 2

Excitation and Emission of N_2^+

2.1 Formation of the N_2^+ Molecule

Production of the N_2^+ molecule is a result of several processes in the upper atmosphere of the N_2 molecule. These processes lead to several electronic states of N_2^+, the ground state $X^2\Sigma_g^+$ (X), and the excited states $A^2\Pi_u$ (A), $B^2\Sigma_u^+$ (B), $D^2\Pi_g$ (D), $C^2\Sigma_u^+$ (C). Excitation to higher states occurs, but those states predissociate rapidly or are excited weakly [*Doering and Goembel*, 1991; *Doering and Yang*, 1996; *Van Zyl and Pendleton Jr.*, 1995]. Also, I have found no evidence in the auroral literature which involves states other than the A and B states. *Van Zyl and Pendleton Jr.* [1995] estimated the fraction of production of states other than the X, A, and B states to be 2 %. Figure 2.1 shows the potential curves for the N_2 molecule and some of its excited states.

Ionization of the N_2 molecule is mainly due to electron impact by primary electrons but also secondary electrons are involved in the ionization process. Other processes also contribute to the ionization, like proton or energetic hydrogen impact, photo-ionization, and chemical reactions including charge exchange reactions. Population of the ion ground state and the excited state depends not only on ionization processes. Cascade transition from a higher excited state to a lower state is a process which needs to be considered. So when considering the production of the N_2^+ molecule and its excited states, we must consider excitation from both the N_2 and N_2^+ ground states, and cascading from higher states. Since we are looking at emissions in the aurora we must also consider de-excitation processes that are of importance as well. Some of the electronic states might dissociate or

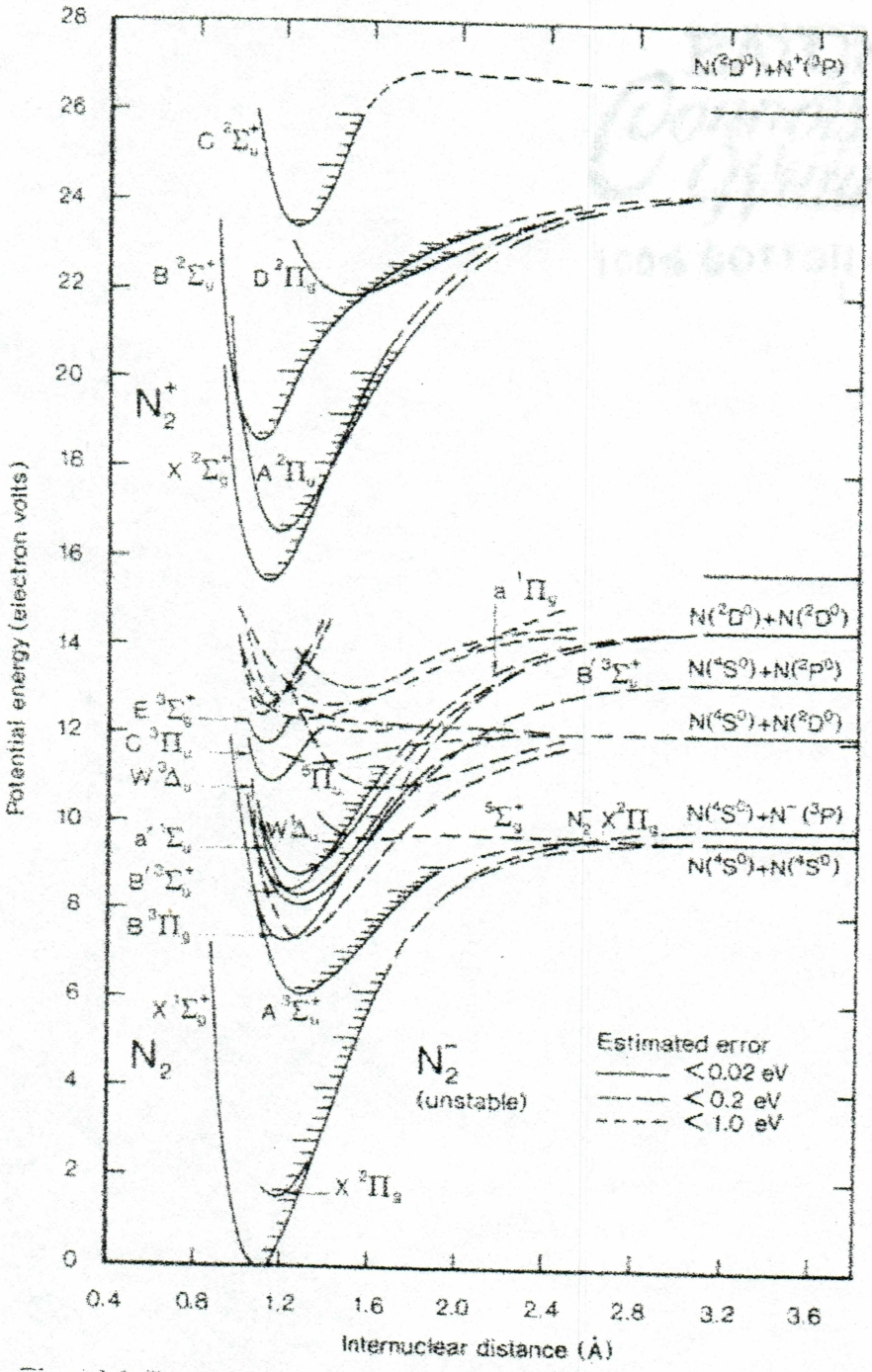

Figure 2.1. Potential curves for the N_2 and N_2^+ including some excited states. From *Rees* [1989].

be de-activated by collisions before they can decay to a lower lying state. Finally, under sunlit conditions, photons can excite the ground state ion (resonant scattering). Thus, the important processes are

- Particle impact by
  - Electrons
  - Protons
  - Neutrals
- Chemical reactions
  - Charge transfer
  - Ion-atom interchange
  - Dissociative processes
  - Collisional deactivation (quenching)
- Cascading
- Photon excitation
- Emission

2.1.1 Particle Impact

Electron Impact

Collision of an incoming electron with N_2 can result in ionization. The process can involve excitation of either a single electron or two electrons from the molecule.

Single electron process : Ionization of an electron with the ion left in either the ground state or an excited state. In general this process has a large cross section and is therefore the most common and most important ionization process. It is characterized by being a direct process with large impact parameter :

$$e + N_2 \rightarrow N_2^+ + e + e \tag{2.1}$$

Two electron process : This process involves excitation of two outer-shell electrons. Two outer-shell electrons are excited simultaneously and the molecule then decays into the ground state ion and a free electron. This process, also known as auto-ionization or Auger effect, contribute very little to the total ionization cross section of N_2.

$$e + N_2 \rightarrow N_2^{**} + e \rightarrow N_2^{+} + e + e \tag{2.2}$$

Excited states can also be created by a similar mechanism which involves two electron excitation, but no decay into the ground state.

Electron Impact is considered the most significant contributor to the ionization of N_2. *Gattinger and Vallance Jones* [1972] and *Gattinger and Vallance Jones* [1973] found from auroral emissions data that the direct electron excitation of N_2 is the major mechanism for production of the A state. Also the ion ground state and the B state is mainly produced by electron impact [e.g. *Vallance Jones*, 1974; *Rees*, 1989]. It should be noted here, that not only incoming primary electrons are important, but also secondary electrons play an important role. Secondary electrons can be produced from other processes than electron impact, e.g. proton aurora, which is caused by incoming beams of protons and hydrogen. The protons can combine with electrons and form neutral hydrogen, which again can be stripped of an electron (see below). Excitation from the ion ground state to higher states by low-energy electrons can also occur. This is a resonance process since the energy of the incoming electron is the same as the re-emitted photon.

Electron impact on N_2 has been studied extensively in laboratories (*Van Zyl and Pendleton Jr.* [1995] and references therein). *Van Zyl and Pendleton Jr.* [1995] did an excellent job in reviewing the previous work done on this subject. Assuming that 98 % goes into the X, A, and B states they inferred the relative production rates of the X, A, and B states. The following is the work described in *Van Zyl and Pendleton Jr.* [1995] and the values are the ones reported therein. It should be noted, that the earlier work used in *Van Zyl and Pendleton Jr.* [1995] is based on emissions of the first negative and Meinel in laboratories, while the work done by *Doering and Goembel* [1991]; *Doering and Yang* [1996] measures the production of the X, A, and B states directly by measuring the primary and secondary electron energies and applying energy conservation.

Early work [*Rapp and Englander-Golden*, 1965] showed that the total ionization cross section for electron impact on N_2 is

$$\sigma_{tot} = \sigma[N_2^+] + 2\sigma[N_2^{++}] + \sigma[N^+] + 2\sigma[N^{++}] = 25.3 \times 10^{-17} cm^2 \tag{2.3}$$

for 100 eV electron impact.

Rapp and Englander-Golden [1965] also reported the fraction of the total ionization cross section resulting in dissociative processes

$$\frac{\sigma[N^+] + 2\sigma[N^{++}]}{\sigma_{tot}} = 0.22 \tag{2.4}$$

Another, and newer result [*Van Zyl and Stephen*, 1994], which is used by *Van Zyl and Pendleton Jr.* [1995], is that the ratio should be 0.25 rather than 0.22.

The ratio between the double ionized and single ionized molecule has been found in two experiments to be 0.018 and 0.014 [*Märk*, 1975; *Halas and Adamczyk*, 1972]. *Van Zyl and Pendleton Jr.* [1995] used the average, thus

$$\frac{\sigma[N_2^{++}]}{\sigma[N_2^+]} = 0.016 \tag{2.5}$$

From the above *Van Zyl and Pendleton Jr.* [1995] obtained a value for the total N_2^+ cross section as 18.4×10^{-17} cm^2. However, when I do the same calculation with the numbers reported in *Van Zyl and Pendleton Jr.* [1995] , I get a value of $\sigma[N_2^+] = 18.7 \times 10^{-17}$ cm^2. Using this value instead and following the work in *Van Zyl and Pendleton Jr.* [1995], the value of the total cross section is

$$\sigma[N_2^+] = 19.2 \times 10^{-17} cm^2 \tag{2.6}$$

This compares to the value given by *Van Zyl and Pendleton Jr.* [1995] of 19.3×10^{-17} cm$^2 \pm 8\%$. These two numbers differ by less than 1 percent and will not influence the work analyzed in *Van Zyl and Pendleton Jr.* [1995].

The production of the three states of interest then becomes

$$\sigma[N_2^+(X)] + \sigma[N_2^+(A)] + \sigma[N_2^+(B)] = 18.9 \times 10^{-17} cm^2 \pm 9\% \tag{2.7}$$

To find the total $N_2^+(B)$ cross section *Van Zyl and Pendleton Jr.* [1995] used an average of previous experiments on the 1N(0,0) emission. Applying the branching ratio for

Table 2.1. Cross section data for the ground state of N_2^+ and the two excited states.

N_2^+ state	Cross section (cm^2)	Partial Branching Ratio	Reference
X	6.05×10^{-17}	0.320 ± 0.147	*Van Zyl and Pendleton Jr.* [1995]
	8.69×10^{-17}	0.448 ± 0.033	*Doering and Yang* [1997]
A	10.11×10^{-17}	0.535 ± 0.112	*Van Zyl and Pendleton Jr.* [1995]
	8.79×10^{-17}	0.452 ± 0.033	*Doering and Yang* [1997]
B	2.74×10^{-17}	0.145 ± 0.019	*Van Zyl and Pendleton Jr.* [1995]
	1.92×10^{-17}	0.099 ± 0.017	*Doering and Yang* [1997]

decay of $N_2^+(B, v' = 0)$ by 1N(0,0) and the Franck-Condon factor for the $N_2(X, v = 0) \rightarrow N_2^+(B, v' = 0)$ transition they obtained

$$\sigma[N_2^+(B)] = 2.74 \times 10^{-17} cm^2 \pm 10\% \tag{2.8}$$

For the Meinel band *Van Zyl and Pendleton Jr.* [1995] again assume the validity of using Franck-Condon factors and using the ratio of the Meinel to 1N band emission ratio they find

$$\sigma[N_2^+(A)] = 10.11 \times 10^{-17} cm^2 \pm 19\% \tag{2.9}$$

Using 2.7 we get the cross section for the ion ground state

$$\sigma[N_2^+(X)] = 6.05 \times 10^{-17} cm^2 \pm 45\% \ . \tag{2.10}$$

The analysis by *Van Zyl and Pendleton Jr.* [1995] can be compared to the more recent work by *Doering and Yang* [1997]. See table 2.1 for a summary of the work by *Van Zyl and Pendleton Jr.* [1995] and *Doering and Yang* [1997].

Thus, we see the large discrepancy between the two. The analysis of *Van Zyl and Pendleton Jr.* [1995] shows that 32 % goes into the ion ground state while as much as 54 % populates the A state. In comparison, the work by *Doering and Yang* [1997] shows a difference of only 4 % between the population of the two states. In both cases, the smallest excitation rate is for the B state. Figure 2.2 shows the cross sections for total ionization

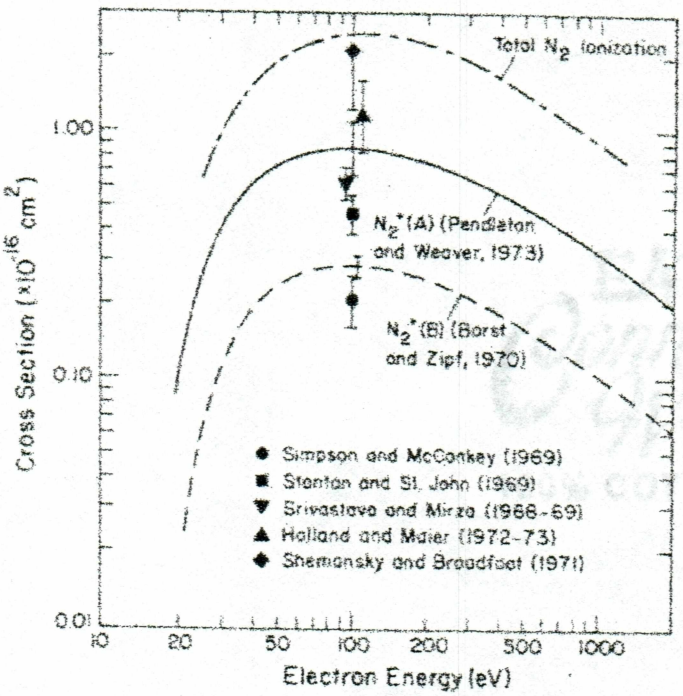

Figure 2.2. Excitation cross section data for total N_2^+, $N_2^+(A)$, and $N_2^+(B)$. From *Cartwright et al.* [1975]. The references listed in the plot are *Pendleton Jr. and Weaver* [1973]; *Borst and Zipf* [1970]; *Simpson and McConkey* [1969]; *Stanton and John* [1969]; *Srivastava and Mirza* [1968, 1969]; *Holland and Maier II* [1972, 1973]; *Shemansky and Broadfoot* [1971]

of N_2, and the N_2^+ A and B states. Notice the similar shape of the cross sections for the three states.

The above discussion focused on particle impact on N_2 forming the states of the ion. The excited states of N_2^+ can also be populated by low energetic electrons impact on the ion ground state. A vibrational enhancement of the first negative band has been explained by impact of low-energetic electrons on N_2^+ in a great red non-sunlit high-altitude aurora [*Degen*, 1981]. In the same work it is concluded that with sunlight present the contribution of this excitation mechanism to the overall enhancement (partly due to resonance scattering) is insignificant. *Henriksen* [1984] observed both night and day-side aurora. The night-side aurora agreed well with the prediction of electron excitation from the neutral ground state while the day-side observations showed some resonance scattering.

Proton and Hydrogen Impact

Protons entering the ionosphere are also a source of ionization and excitation of the ambient molecules. When entering the ionosphere the protons are constrained to move along the magnetic field lines. However, there is a possibility that a proton can capture an electron, forming a neutral hydrogen and thus are free from the constrained motion. During a proton aurora we must then consider ionization from both protons and hydrogen atoms. Two processes are relevant for the proton interaction [e.g. *Vallance Jones*, 1974; *Rees*, 1989]

1) Ionization collision :

$$H^+ + N_2 \rightarrow H^+ + N_2^+ + e \tag{2.11}$$

2) Charge-exchange collision :

$$H^+ + N_2 \rightarrow H + N_2^+ \tag{2.12}$$

The ionization process dominates for high proton energies while the electron-capture process dominates at lower energies [*Van Zyl et al.*, 1983]. The maximum cross sections for the two processes are in the order of $\sigma \approx 10^{-15}$ cm^2 [*Vallance Jones*, 1974] and [*Rees*, 1989] for 10 keV protons while *Van Zyl et al.* [1983] found $\sigma \approx 10^{-16}$ cm^2 for the 1N(0,0) band emission. Other investigations also involves the first negative band [e.g. *Rees*, 1982; *Van Zyl et al.*, 1984]. I have found nothing on Meinel emissions from proton impact in the literature and the possibility that either the B state is favorable excited by proton impact compared to the A state, or vice versa, must be considered.

For impact with neutral hydrogen two collisions are relevant [*Vallance Jones*, 1974; *Van Zyl et al.*, 1984]

$$H + N_2 \rightarrow H + N_2^+ + e \tag{2.13}$$

$$H + N_2 \rightarrow H^+ + N_2^+ + 2e \tag{2.14}$$

Impact with neutral hydrogen has been reported by [*Van Zyl et al.*, 1983]. They found a cross section for the 1N(0,0) emission for $H + N_2$ collisions to be in the order of $3 \cdot 10^{-17}$

cm^2 for 10 keV impact. Work done by others referred in *Van Zyl et al.* [1983] indicates a cross section for total ionization of N_2 by H impact to be in the order of $5 \cdot 10^{-16}$ cm^2. As was the case for proton impact, nothing has been found involving Meinel emission resulting from hydrogen impact.

We see that the cross sections for production of N_2^+ by proton/hydrogen impact are of the same order as for electron impact. Thus, if there is proton precipitation into the ionosphere we must take this into account when discussing the excitation of N_2^+.

2.1.2 Charge Transfer

Charge transfer is a chemical process which can give rise to simultaneous ionization and excitation of molecules in the atmosphere, and the process is both a source and sink of the N_2^+ molecule . It is characterized by the processes

Source :

$$A^+ + N_2 \rightarrow N_2^+ + A \tag{2.15}$$

Loss :

$$A + N_2^+ \rightarrow N_2 + A^+ \tag{2.16}$$

where A indicates an atmospheric species.

Charge transfer is still an open research topic in production of N_2^+ since it was postulated by *Omholt* [1957]. In his work he proposed the reaction

$$O^+(^2D;^2P) + N_2(X^3\Sigma) \rightarrow O(^3P) + N_2^+(A^2\Pi), \tag{2.17}$$

as a possible source of the $N_2^+(A)$ state. According to *Fox and Dalgarno* [1985] it can populate vibrational levels in both the $N_2^+(X)$ and $N_2^+(A)$ states to $v = 5$ and $v = 1$, respectively. However, this work was done for the non-auroral daytime terrestrial ionosphere. The reaction has been studied intensively and appears to play an important role in the dayglow, but its role in the aurora has not yet been determined. Since it favors the $v = 1$ level of the $N_2^+(A)$ state, an increased intensity of transitions involving $v = 1$ is expected. *Gattinger and Vallance Jones* [1973] examined the $\frac{(1,2)}{(0,1)}$ ratio and found no evidence of an additional population of the $N_2^+(A)$ state other than population by electron impact. On the other hand, *Espy et al.* [1987] found strong evidence for the contribution of the charge

transfer process. If the charge transfer process is occurring in aurora we would also expect the ratio of $\frac{M}{1N}$ to change. This thesis involves the Meinel (2,0) emission, which should not be affected by the charge transfer discussed above.

Loss of N_2^+ by charge transfer processes are [e.g. *Rees*, 1989; *Vallance Jones*, 1974]

$$N_2^+ + O_2 \rightarrow O_2^+ + N_2 \tag{2.18}$$

$$N_2^+ + O \rightarrow O^+ + N_2 \tag{2.19}$$

$$N_2^+ + NO \rightarrow NO^+ + N_2 \tag{2.20}$$

The importance of these reactions can be estimated. The ion-neutral collision frequency in the E and F-region (90 - 160 km and 160 - 500 km) are of the order $2 \cdot 10^3 - 10^2$ s^{-1} and $0.5 - 0.05$ s^{-1}, respectively[1]. The lifetime of the A and B state are in the order of 10^{-6} s and 10^{-9} s, respectively. The two states decay to the ground state before any collision can occur and the above reactions are only important for the ion ground state. Thus, when considering emissions from the A and B state we can neglect the above reactions.

2.1.3 Ion-atom Interchange

The ion-atom interchange

$$N_2^+ + O \rightarrow NO^+ + N \tag{2.21}$$

is a loss mechanism for N_2^+ [e.g. *Rees*, 1989; *Vallance Jones*, 1974]. However, as described above, this process only involves the ion ground state and has no influence on the emissions from the A and B state.

2.1.4 Dissociation

One dissociation process of interest is the dissociative electron-ion recombination [e.g. *Rees*, 1989; *Vallance Jones*, 1974]

$$N_2^+ + e \rightarrow N + N \tag{2.22}$$

Zipf [1980] studied the dissociative process for the ion ground state, and the listings by *Vallance Jones* [1974] and *Rees* [1989] indicate that only the ion ground state is influenced

[1]Plasma Formulary, Naval Research Laboratory (NRL) by J. D. Huba, 1994

by this process. However, more recent work by *Oddone et al.* [1997] shows that the $A(v = 1)$ state is dissociated as well. No other vibrational levels dissociate. Unfortunately, they were not able to determine rate constants. Since it has not been reported as a loss of the A state in the auroral literature we will assume that the dissociation of the A state is small and that only the ion ground state is dissociated. Thus, the dissociative recombination should not influence the emissions studied here.

2.1.5 Quenching

Quenching or collisional deactivation is important for excited species with a long radiative lifetime. Emissions from metastable states are limited by deactivation through collisions with other species. The reaction is

$$N_2^+(*) + A \rightarrow N_2^+ + A \tag{2.23}$$

where $*$ indicates an excited state. If quenching is negligible then the metastable state can radiate.

Of the two emissions of interest only the $N_2^+(A)$ state has a lifetime long enough for quenching to be a factor ($\tau \approx 10$ μs) [e.g. *Vallance Jones*, 1974; *Holland and Maier II*, 1972]. The $N_2^+(B)$ state have lifetime of 70 ns and a quenching height near 48 km [*Vallance Jones*, 1974]. *Cartwright et al.* [1975] concluded that the most important quenching particles are N_2 and O_2 and found that quenching is important for altitudes less than 120 km, and the quenching height (altitude where one-half of the molecules have been de-activated) to be approximately 85 km. *Vallance Jones and Gattinger* [1978] investigated the quenching effect in three types of aurora, lower-altitude, normal-altitude, and high-altitude aurora and found that the low-altitude aurora was 20 % weaker than the normal-altitude aurora. Newer work, [*Piper et al.*, 1985], concluded that a 20 % reduction of the Meinel band corresponds to a height of approximately 95 km while *Espy et al.* [1987] found that the quenching rate is less than 1 % for altitudes above $\approx$ 105 km. Figure 2.3 shows the altitude profile versus the Meinel and first negative ratio. The dependence illustrates the quenching effect of the Meinel band.

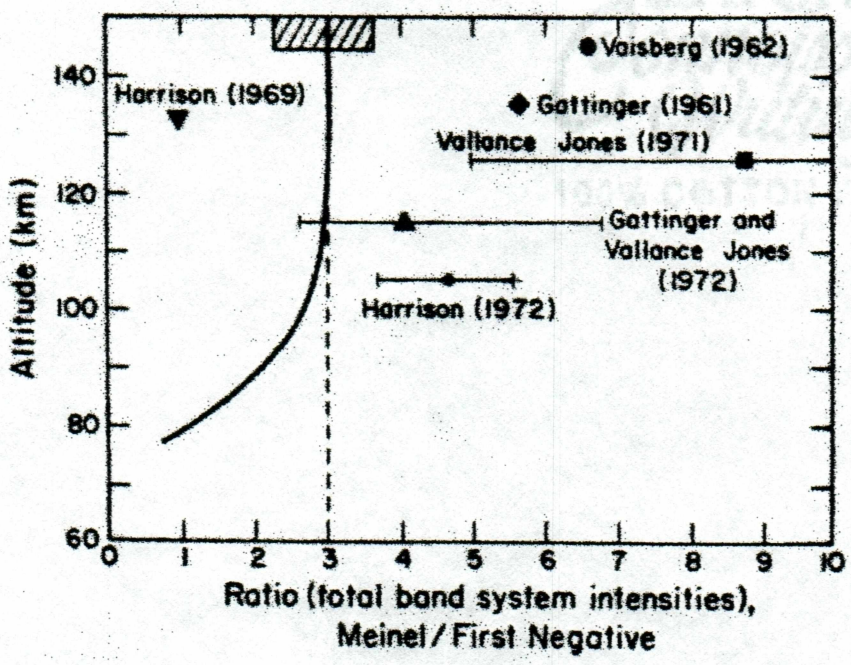

Figure 2.3. Altitude profile of the total Meinel/first negative ratio. The dashed line indicates the result without quenching of the A state. From *Cartwright et al.* [1975]. The references listed are *Harrison* [1969, 1972]; *Vallance Jones* [1971]; *Gattinger and Vallance Jones* [1972]; *Vaisberg* [1962]; *Gattinger* [1961].

2.1.6 Cascading

Cascading effects are a common factor in excitation and de-excitation processes. If cascading to the states of interest occurs it will increase the population and hence increase the emission. Cascading occurs when the molecules are excited to a higher level i above the level of interest j and radiative transitions $i \rightarrow j$ may occur. Thus, cascade transitions increase the population of the j state and need to be taken into account when discussing the population of the different states and their emissions. Cascading processes can be written as

$$N_2^+(i) \rightarrow N_2^+(j) + h\nu \tag{2.24}$$

where $h\nu$ is the energy of the emitted photon.

We are observing the emissions originating from the A and B states and are therefore interested in knowing if those states can be populated by cascade. States above the A and B states are either weakly excited or predissociate quickly. Additional population of the A and

B state by cascading is thus negligible [e.g. *Fons et al.*, 1994; *Van Zyl and Pendleton Jr.*, 1995; *Goembel et al.*, 1994; *Doering and Yang*, 1996].

2.1.7 Resonance Scattering

Resonance scattering occurs when an incoming photon excites the molecule and the molecule then re-emits a photon with the same energy. During sunlit conditions the N_2^+ ground state can be excited to the A or B state, and then decay back to the ion ground state by emission in the Meinel band and first negative band, respectively.

$$N_2^+(X) + h\nu \Leftrightarrow N_2^+(A, B) \tag{2.25}$$

As mentioned earlier, *Henriksen* [1984] observed both night and day-side aurora. The day-side observations indicated resonance scattering as a major mechanism of the first negative bands with about 40% of the emission being due to resonant scattering. This is in agreement with *Broadfoot* [1967]. Both searched for an enhancement of the Meinel band due to resonance scattering but found none. *Henriksen* [1984] predicted the g-factor of the Meinel (2,0) and first negative (0,1) to be 2.5×10^{-4} and 1.3×10^{-2}, respectively. The g-factor is defined as the number of photons which are resonance scattered per second by a particular transition of the molecule which is illuminated by unattenuated sunlight [*Broadfoot*, 1967]. Based on the g-factors, *Henriksen* [1984] predicted that no detectable Meinel (2,0) emission due to resonance scattering should be found in his observations.

2.2 Emission

Transition in the N_2^+ molecule result in some of the most prominent emissions in the aurora. The first negative band $B^2\Sigma_u^+ \rightarrow X^2\Sigma_g^+$ and the Meinel band $A^2\Pi_u \rightarrow X^2\Sigma_g^+$ are both dominant features in the blue and near-infrared wavelength region, respectively. Before going into detail of the two emissions, let us consider the other states of N_2^+. The next excited states above the $B^2\Sigma_u^+$ are the $C^2\Sigma_u^+$ and $D^2\Pi_g$ states. Higher lying states are produced, but are too weakly excited or dissociate too quickly to have any significant emissions [e.g. *Van Zyl and Pendleton Jr.*, 1995; *Doering and Yang*, 1996]. The transition

between the B and A states $B^2\Sigma_u^+ \rightarrow A^2\Pi_u$ is electric dipole forbidden. The $C^2\Sigma_u^+ \rightarrow X^2\Sigma_g^+$ (second negative) is allowed by electric dipole transition and extends from 1377 to 2100 Å [*Ajello*, 1970]. However, the production cross section for the C state is small and most of the state predissociates to N^+ and N [*Van Zyl and Pendleton Jr.*, 1995; *Fons et al.*, 1994; *Ajello*, 1970; *Doering and Yang*, 1996]. The $D^2\Pi_g \rightarrow A^2\Pi_u$ (Janin-d'Incan band) occurring in the range 2000 - 3100 Å has been studied by *Fons et al.* [1994]. The emission cross section observed was of the order of 10^{-20} cm^2. Thus, the transition is very weak and should not influence the analysis here. In fact, *Piper et al.* [1986] did not observe any detectable signal from this emission.

The two remaining emissions are the first negative and Meinel emissions. Production of the A and B states by electron impact on N_2 involves the same kind of one-electron ionization process [*Fons et al.*, 1994]. Based on that, one might expect the shape of the excitation cross sections to be similar. This is confirmed by *Cartwright et al.* [1975] and *Fons et al.* [1994]. Figure 2.4 illustrates the similar shapes.

The similar shapes of cross section data turns out to be useful when we consider the ratio between the two emissions. The intensity of an electronic band is defined as

$$I(v' \rightarrow v) = N(v')A(v' \rightarrow v) \tag{2.26}$$

where $N(v')$ is the population in the v'th level of the upper state and $A(v' \rightarrow v)$ is the Einstein coefficient for the transition between this level to level v in the lower state (the ion ground state). Since the excitation cross sections for the A and B states are similar for electron impact, we expect a constant ratio between the two populations. Thus, the intensity ratio between the two transitions is a constant provided only excitation by electron impact are important

$$\frac{I_M(v' \rightarrow v)}{I_{1N}(v''' \rightarrow v'')} = constant \tag{2.27}$$

where v' and v''' indicate the levels of the upper states, and v and v'' are levels of the lower state. The two transitions presented here are the Meinel (M) (2,0) and first negative (1N) (0,1), so we have that

$$\frac{I_M(2,0)}{I_{1N}(0,1)} = constant \tag{2.28}$$

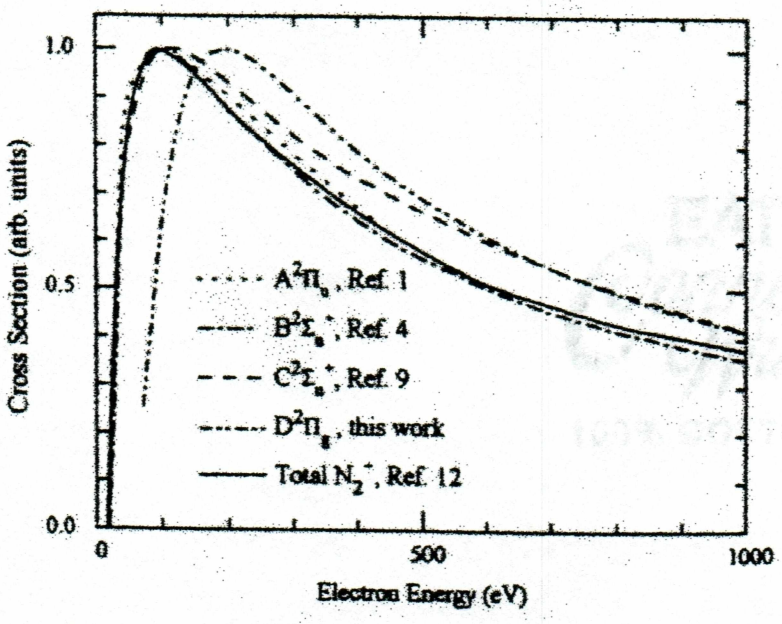

Figure 2.4. Cross section curves for the N_2^+, and the lower lying excited states. The similar shapes for the A, B, and D states are clear. The different shape of the C state might be due to a different ionization process than the one involved for production of the A, B, and D states. From *Fons et al.* [1994]. The references listed are *Stanton and John* [1969] (ref.1), *Borst and Zipf* [1970] (ref.4), *van de Runstraat et al.* [1974] (ref. 9), and *Itakawa et al.* [1986] (ref.12).

2.3 Summary

The N_2 molecule can be ionized and produce N_2^+ in various states. Most of this production goes into the ion ground state, X, and the two excited states A and B. The major mechanism in the production is electron impact on the neutral molecule. If proton precipitation is present it also contributes significantly. The emissions studied here are not influenced by charge transfer processes and will not be affected by any of the chemical reactions other than quenching in case of a strong aurora, in which case the altitude of the aurora is close to the quenching height for the A state. Additional population of the A and B state by cascading is negligible. If the aurora is sunlit resonance scattering will affect the population with the B state being preferable populated over the A state. If electron impact is the only source of the A and B states we will expect the ratio of the emission between the Meinel

(2,0) and first negative (0,1) to be constant.

Chapter 3

Instrumentation

3.1 The Imaging Spectrograph

The instrumentation system used in this experiment consists of an imaging spectrograph build by J. Baumgardner, Boston University, a video digitizer/framegrabber, and a PC (see figure 3.1, 3.2, and 3.3). In the configuration used here [*Semeter*, 1997], the light enters a 100 mm f/3.5 entrance objective followed by a 0.2 mm-wide 40 mm-long slit entrance and a field lens (75 mm focal length, and 60 mm diameter). The beam is then made parallel by a 340 mm, f/3.4 collimator before it illuminates a 600 lines/mm diffraction grating. The detector is a 85 mm f/1.2 lens followed by an image intensifier with a photon gain on the order of 5000, two lenses (135 mm, f/2.8 and 50 mm, f/1.2, respectively), and finally a Pulnix TM-745 high resolution CCD camera with a standard shutter speed of 1/30 s. The two lenses placed after the intensifier reduce the image from the intensifier to fit the CCD. The resolution of the imaging spectrograph depends on the grating, dimensions and locations of the detector elements, aberrations in the image, and the magnification of the image. Most of these parameters are not known and the resolution cannot be calculated for the imaging spectrograph. However, the resolution can be estimated by finding the half-width of an atomic emission line. Using an Argon gas discharge lamp the spectral resolution of the imaging spectrograph is estimated to be 16 Å.

The entire wavelength region of interest (blue to red) cannot be detected at once. This is solved by letting the grating be mounted on a rotating table and then scan the wavelength region from the blue spectrum to the red. The rotating table is turned by a stepping motor

controlled by a computer. This way, the instrument divides the visible spectrum into 6 regions centered around 4200, 4800, 5600, 6300, 7000, and 7700 Å.

3.2 Data Acquisition and Software

The data acquisition is made through a Matrox Meteor II digitizer/framegrabber on a Micron Pentium II 400 MHz PC running Windows NT as operating system (OS). Besides the digitizer, the computer system controls the on/off switch on the intensifier, the integration time on the CCD, and the stepping motor to rotate the grating plate. The operation of the parts build into the instrument assembly (intensifier, CCD, and stepping motor) is done through a Scientific Solution base board, which enables digital input/output to and from the computer. However, Windows NT does not allow the user to execute I/O instructions from a user program. A software package (WinRT-VB) is applied to allow port I/O and memory I/O to be handled from a user program. The program to control the entire system is a Visual Basic program. The user is able to change wavelength channel (rotating the grating table), turn the intensifier on/off, and determine the integration time (in frames) on the CCD. The integration time can be set to a specific number of frames and the CCD keeps the shutter open while reading out empty frames until the desired number of frames has been reached. The program then closes the shutter, and the next frame being read out is the accumulated frame which is been captured by the framegrabber. In order to capture the accumulated signal, an event controller is applied to count each frame read out from the CCD camera. The event controller is build-in software coming with the digitizer/framegrabber, Active Matrox Imaging Library Lite (ActiveMIL Lite), and integrates into Visual Basic. By keeping track of the number of empty frames read out the software can then grab the accumulated signal.

The size of the captured image is 640 $\times$ 480 pixels with 256 graylevels (8 bits) per pixel. The video depth of 8 bits sets the upper limit for how strong a signal one can obtain before the image is oversaturated. It is useful to be able to determine when an image is oversaturated. This is done by applying a color code to the image when a certain pixel value is reached. In the data used in this analysis, a yellow color code is applied when a pixel has a value of 250 or higher. In this way the user can determine when an image is

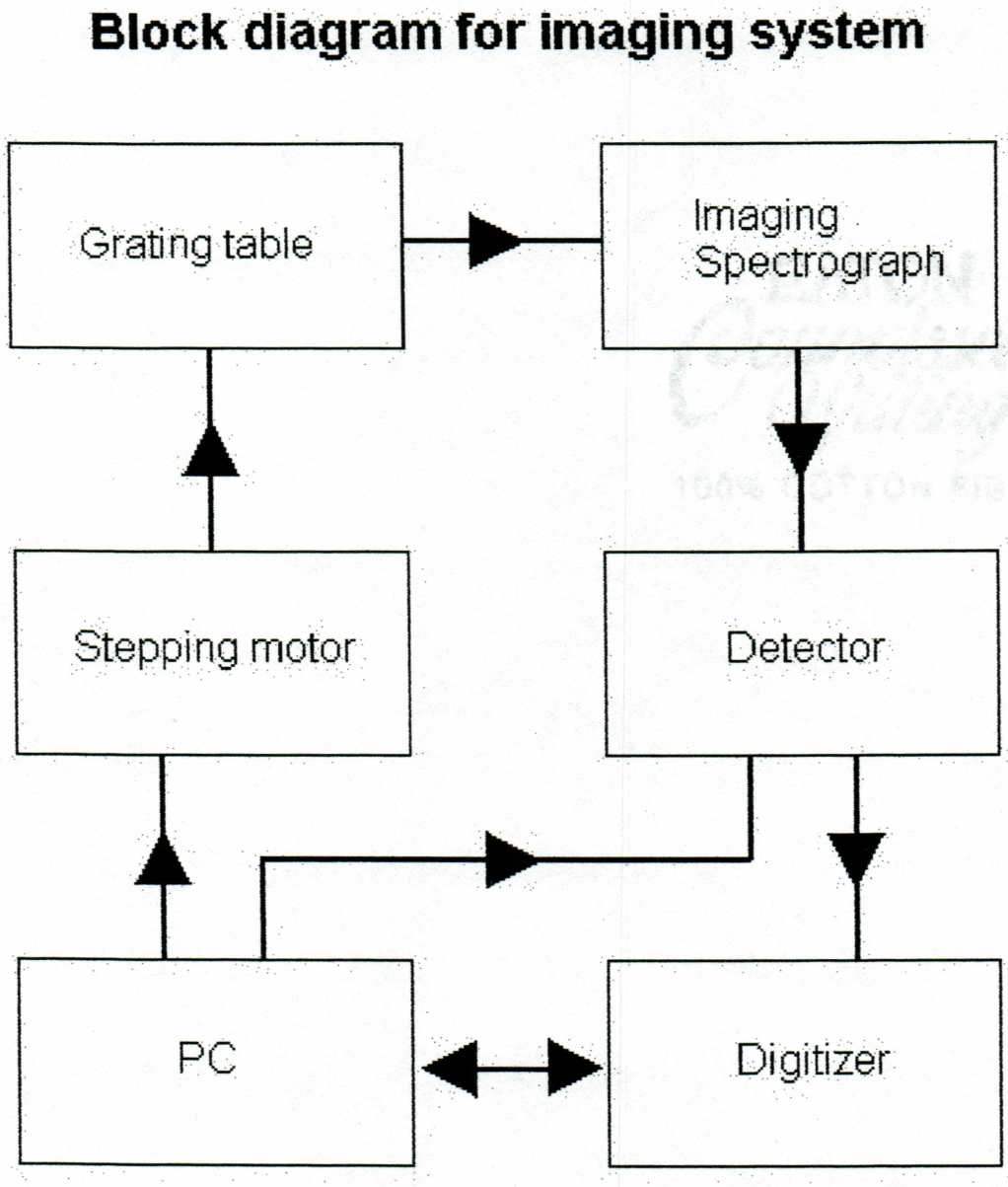

Figure 3.1. Schematic block diagram of the experiment set-up.

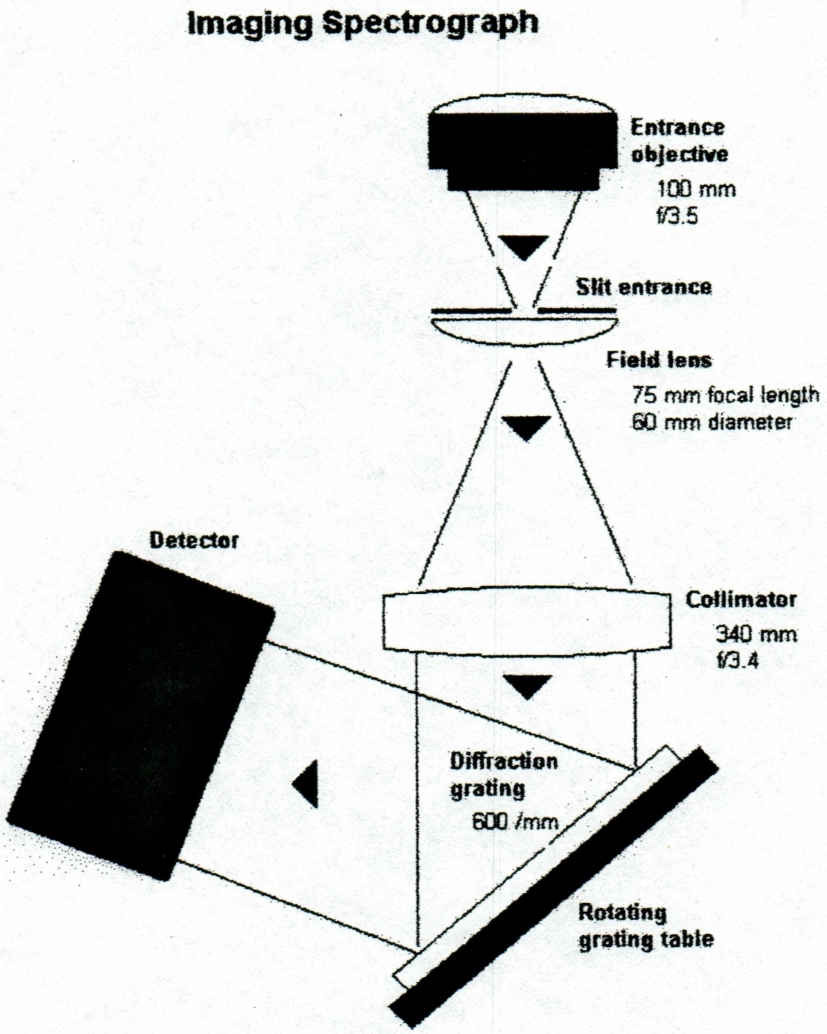

Figure 3.2. Schematic of the imaging spectrograph. The detector is shown in next figure. Redrawn from *Semeter* [1997].

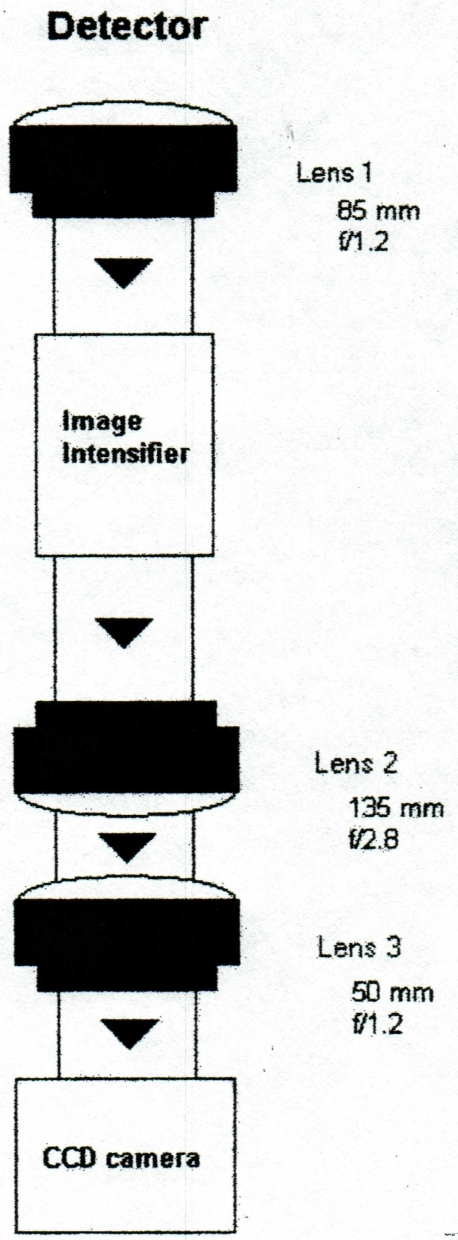

Figure 3.3. Schematic of the detector used in the instrument. Redrawn from *Semeter* [1997].

oversaturated and adjust the integration time to an appropriate setting.

Last, the user can determine how many images to be recorded in sequence in the same wavelength window. The purpose of this is to later co-add (stack) the images. One reason for co-adding is that, if low light level conditions are present, stacking several images together enhance the signal and at the same time reduces any random signal (noise) in the image. Another reason is to increase the signal-to-noise ratio. If one adds several signals, $N_1 + N_2 + \ldots$, the noise only adds up as $\sqrt{N_1 + N_2 + \cdots}$, thus increasing the signal-to-noise ratio.

Each individual frame is stored on a hard disk and co-adding can then be done at any later time. The program obtaining the images could have done the co-adding real-time. However, the advantage of doing so later is to be able to investigate each frame for eventual features that might change during one sequence, e.g. fast moving aurora, pulsating aurora, or a star passing through the instruments field-of-view. Since the images need to represent the *same* aurora the above features should not be present. By looking at the individual frames these features can be excluded.

Chapter 4

Processing of Data

4.1 Calibration of Data

Before any scientific conclusions can be made, the data must be calibrated. In our study, we must consider errors introduced in the electronics, optical effects, additional unwanted emission sources and relate our data values to quantities that can be used to reach our goal. Figure 4.1 shows an example of a raw image obtained from the imaging spectrograph. The figure shows a spectra in the 7000 Å window. The spectral lines are slightly curved as a result of diffraction from the grating. It is also clear from the image that the spectral region does not fill the entire image field of the CCD.

In this study we must correct for :

Read-out noise : The signal from the sensor is amplified, converted to voltage pulses and finally digitized through an A/D converter before it is read out in computer-readable format. Any contribution to the signal throughout this process will be digitized together with the signal accumulated onto the sensor. The additional unwanted signal is the read-out noise. It is only added to the signal during the read-out process, not during the accumulation of signal during an exposure. Thus, read-out noise is independent of integration time.

Dark Current : Due to thermal emission additional electrons can be generated and give rise to *dark current* which is a cause of noise in data. Even with no illumination on the CCD it will be filled if exposure time is long enough. Thus, dark current is

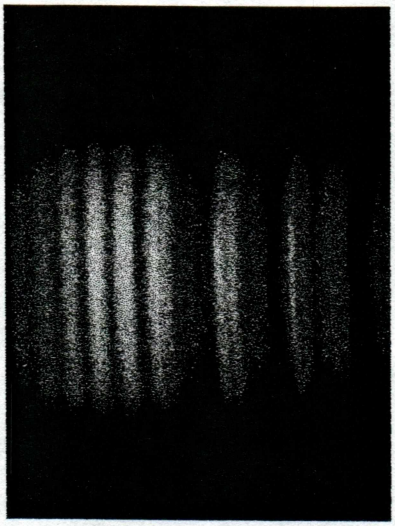

Figure 4.1. This image, showing the auroral spectra in the 7000 Å window, illustrates a typical raw data image. The wavelength is increasing from left to right with 7000 Å being near the center of the image. The vertical dimension is the spatial dimension.

independent of incoming light, but dependent of the integration time and temperature.

CCD defects : Some light sensitive elements on the CCD may be defective and cause an erroneous measurement. This is a static effect independent of incoming light and integration time.

Curvature effect : An optical effect in the instrument which result in curved emission lines as seen by the detector. This is a natural consequence of diffraction from the grating for rays that originate off the grating normal.

Vignetting effect : Vignetting is an optical effect which comes from the geometry of an objective lens. The effect is a decrease in intensity away from the optical axis. Light entering the lens near the optical axis has a larger cross section of projection onto the the second lens in the instrument while light entering under a larger angle has a smaller cross section and thus less light enters the second lens near the edges. Thus the image appears dimmer at the edges. Figure 4.2 shows an example of the vignetting effect.

Background : Random signals coming into the system from a variety of external sources are classified as background signal. The most common sources for auroral studies

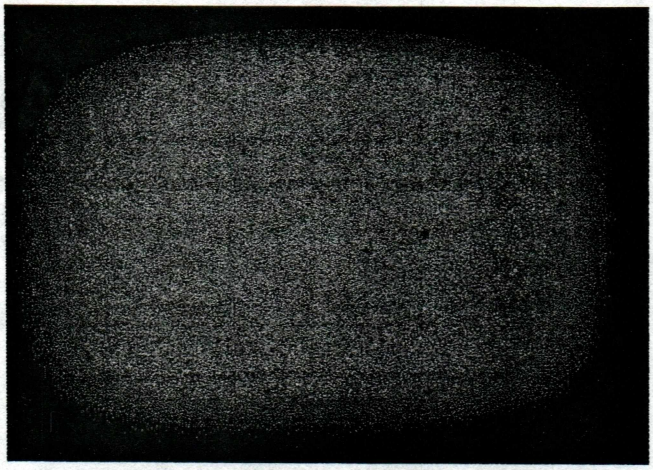

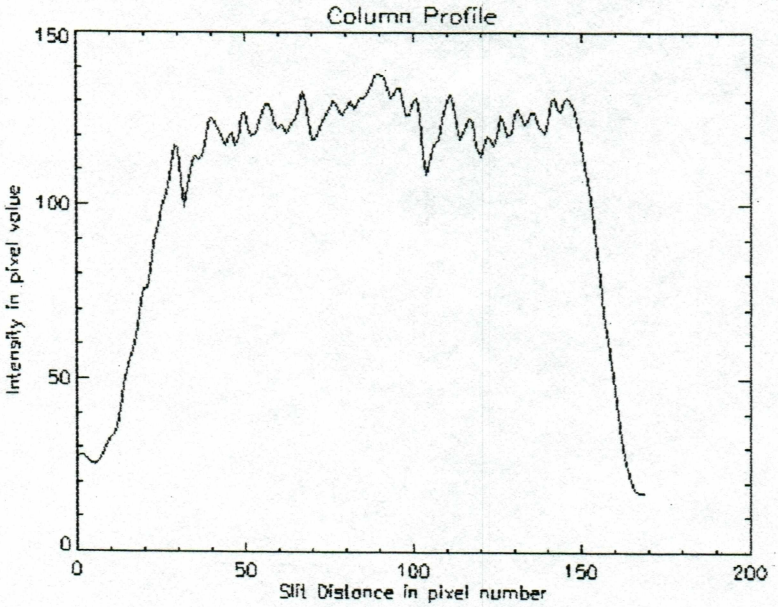

Figure 4.2. The image shows a spectrum obtained with a standard lamp. The lamp emits at all wavelengths and the image should be uniform in the direction of the slit (vertical dimension in image). The plot shows a column profile from the center part of the image. The vignetting is shown as a slow drop in intensity towards the edges. The steep drops in intensity at the edges is not vignetting but merely shows the limit of the projected image, in other words, the projection does not fill the CCD's field.

are the sky background and nightglow. Thus, background signal is dependent of integration time.

Wavelength Calibration : The raw data image shows the line spectra of the aurora as a function of pixel number which ranges from 0 to 239 (size of image in wavelength direction). Wavelength calibration facilitates the conversion from pixel number to wavelength.

Absolute (intensity) Calibration : In raw form the intensity is given in pixel value and ranges from 0 - 255. These values need to be calibrated to give a physical quantity according to the spectral response of the instrument, e.g. photons/(m^2·s). The CCD is merely a counting device counting the photons incident on the CCD. Since the energy of a photon vary with its wavelength we need to attribute the correct energy to the photons incident on the CCD by doing an absolute intensity calibration.

Atmospheric corrections : Between the source of the emissions and the observing instrument is the atmosphere. In order to relate the observed brightness to the emission the data has to be corrected for scattering and absorption through the atmosphere.

4.1.1 Calibration for Read-out Noise

The read-out noise can be determined by extrapolating the dark-current data (see below) to zero integration time (corresponding to a frame without any data accumulated). The signal obtained must then entirely come from the electronic equipment. Figure 4.3 shows the plot of read-out noise and dark-current. The read-out noise was found to be 1.09 counts per pixel, and needs to be subtracted from the original image.

4.1.2 Calibration for Dark Current

Dark current correction is made by taking several images with no incoming illumination (this is done by keeping a lens cap on the entrance objective) over different exposure times. The signal received contains both the dark current and the read-out noise. Figure 4.3 shows the dark-current plus read-out noise as a function of integration time (in frames). A linear dependence with integration time is found. The read-out noise is then subtracted from

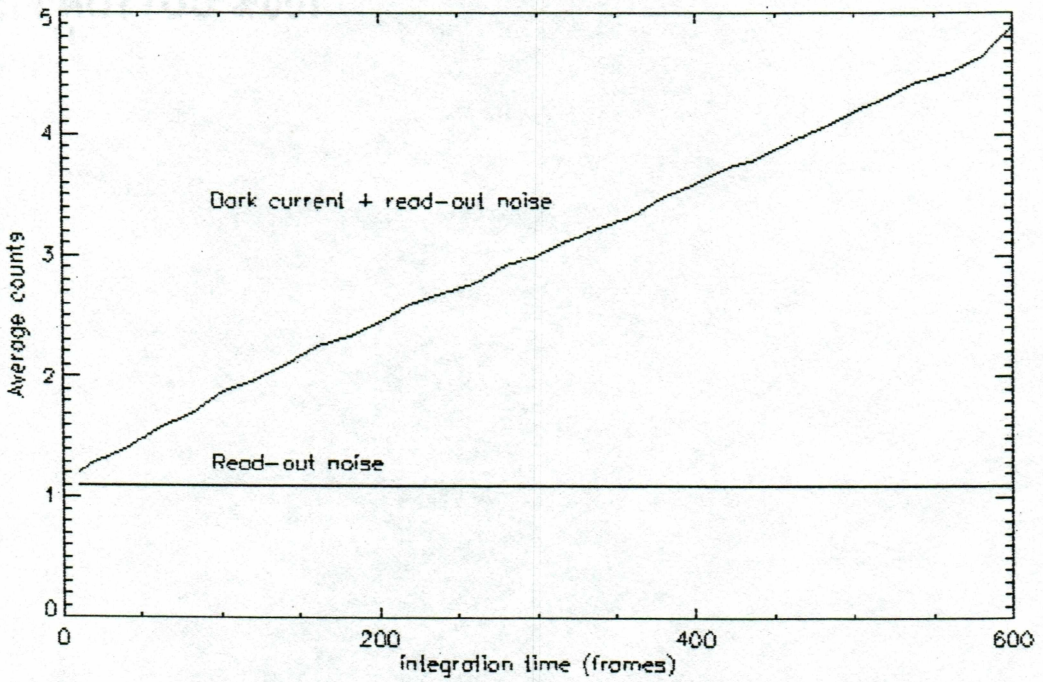

Figure 4.3. The average dark current per pixel plus read-out noise as a function of integration time (in frames). The read-out noise is constant and are determined as the signal obtained with zero integration time.

the combined signal and a pure dark current function is obtained. The integration time of an image is being used to interpolate the dark current to obtain a dark current value corresponding to that specific image. The found value is then subtracted from the original image.

4.1.3 Calibration for CDD Defects

There are two ways a pixel can be defective. It can be reading a constant value at all times. These pixels can be found be illuminating the entire CCD and varying the intensity. A "dead" pixel will always be dark, while a "bright" pixel always will be bright. No such pixels was observed in the region of the CCD where the data are analyzed. The other way a pixel can be defective is by systematic reading a wrong value, e.g. 5 counts too high. It is difficult to know if such pixel exist. Data taken with no light source illuminating the camera shows values ranging from 0 to approximately 5. But one cannot tell if those values are due to thermal electrons (dark current). However, by averaging over several rows in the image the influence of defective pixels should be minimized. Also, by making a flatfield correction (see description under *Calibration for Vignetting Effects*) the defective pixels will be corrected to give the average value.

4.1.4 Calibration for Curvature Effect

The image produced from the slit is not straight but rather parabolic and the image is wider near the center than at the ends[1]. The curvature of the emission lines are then a natural consequence of diffraction for rays that originates above or below the plane that contains the grating normal and is perpendicular to the grating rules. Mathematical it is shown by the full grating equation

$$\frac{n\lambda}{d} = (\sin\alpha + \sin\beta) \cdot \cos\theta, \tag{4.1}$$

where n is the order of diffraction, d is the groove spacing, α is the angle of incident, β is the diffraction angle, and θ is the angle subtended by the slit.

We can avoid the curvature effect in our case since we are only interested in auroral intensity along magnetic zenith. This region is limited to the very center of the data images

[1]Private communication, Jeffrey Baumgardner, Boston University

and by reducing the images to this center part we can neglect curvature effects. By doing this we are also reducing the vignetting effect along the slit and could in practice neglect it. However, for a general purpose the vignetting along the slit is still being calibrated for. Figure 4.4 shows an example of a reduced image.

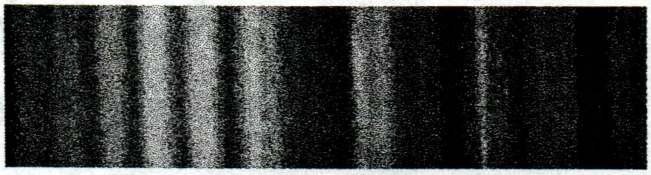

Figure 4.4. The actual image for further analysis after being reduced to a narrower image, and thus neglecting curvature effects. The magnetic zenith is the center of the image in the wavelength direction.

4.1.5 Calibration for Vignetting Effects

A standard lamp with a known spectral response (black body radiation at a known temperature) was used. The standard lamp illuminated a Lambertian surface[2]. The instrument was aligned towards the surface in such way that the surface covered the entire field of view. In theory the image produced should then be uniform in the slit direction and fit a black body radiation curve in the wavelength direction. Due to vignetting effects and the intensifiers spectral response that is not the case. For the vignetting effect a correction is made such to fit the signal to the known emission (a flatfield correction/image). The calibration was done separately in the direction of the slit and in the direction of wavelength.

Along the slit

Along the slit the illuminated screen should have no intensity variations. However, due to an intensity drop-off away from the optical axis the intensity is not uniform in the slit direction. Standard lamp data can be used to correct for this. The center of a standard lamp image represent the intensity that should be present throughout the image in the slit direction. We want to correct the edges such that the image appears uniform in the slit direction. 5

[2]A Lambertian surface is an ideal diffuse surface obeying Lambert's cosine law which means that the luminance of the surface is the same regardless of the viewing angle.

different standard lamp images was recorded. For each image a section which represented the average intensity signal was chosen. The median for that part was determined and used to normalize the image. Inverting the normalized image and averaging over several images gives the final flatfield image. Dividing the original image by the flatfield image calibrates for the vignetting effect along the slit and results in a uniform image in the slit direction.

Let X_i be the i'th standard lamp image, then the normalized images is

$$X_{i,norm} = \frac{X_i}{median(X_i)}. \tag{4.2}$$

The i'th inverted image is the inverse of the normalized image

$$X_{i,flat} = \frac{median(X_i)}{X_i}. \tag{4.3}$$

The total flatfield image is obtained by summing over all images and averaging

$$X_{flat} = \frac{\sum X_{i,flat}}{N}. \tag{4.4}$$

The data image is then divided by the flatfield image such that the spectral response is uniform in the direction of the slit.

Wavelength direction

A pure vignetting correction in the wavelength direction is not possible due to the non-uniform spectral response of the intensifier. This calibration is therefore done together with the absolute intensity calibration. See the section for absolute intensity calibration for further details.

4.1.6 Wavelength Calibration

Gas discharge lamps were used for the wavelength calibration. Helium, Argon, and Krypton lamps were used and provided well-known lines in the spectral region 3900 - 8000 Å. Each wavelength window was then represented by two or more lines from the above lamps. By knowing the wavelength of two lines in a window, λ_1 and λ_2, and their corresponding pixel position (number), X_1 and X_2, we can determine the relationship between wavelength and pixel position. We will assume the relationship is linear, that is, the linear dispersion is

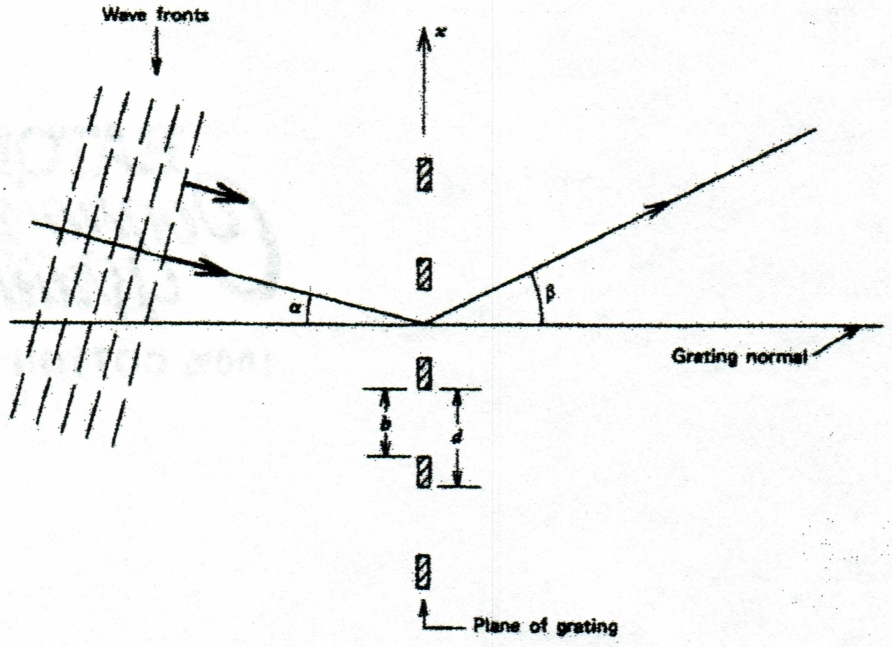

Figure 4.5. An incoming beam of light incident on a diffraction grating. From *Gray* [1992].

constant. The validity of this assumption can be shown if we consider an incoming beam on a diffraction grating (figure 4.5).

If the incident angle is α, the angle of diffraction is β, and the slit spacing is d. For simplicity let us consider rays that are in the grating normal plane, then the grating equation is

$$\frac{n\lambda}{d} = \sin\alpha + \sin\beta, \tag{4.5}$$

where n is the order, λ is the wavelength (same units as d). The angular dispersion then becomes

$$\frac{\partial\beta}{\partial\lambda} = \frac{n}{\cos\beta \cdot d}. \tag{4.6}$$

If we combine the angular dispersion from the grating with the focal length of a camera we can find the linear dispersion.

Referring to figure 4.6 we have a camera with a focal length f and two beams leaving the grating having wavelength λ and $\lambda + d\lambda$ and an angle difference $d\beta$, incident on the

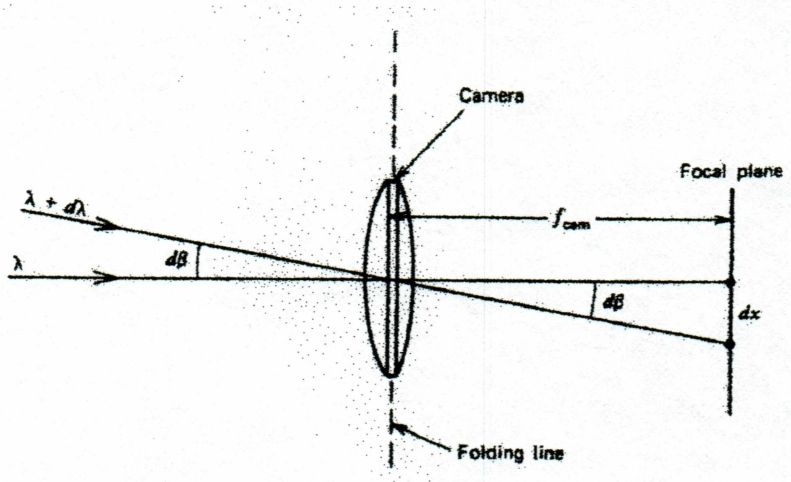

Figure 4.6. Two beams of light entering a camera. This figure is shown to help illustrate the constant linear dispersion. From *Gray* [1992].

camera. Then the linear separation in the image is

$$dx = f d\beta, \tag{4.7}$$

and the linear dispersion is

$$\frac{d\lambda}{dx} = \frac{\cos\beta}{n \cdot f}. \tag{4.8}$$

If β is small, the linear dispersion is constant. Thus, for first order (n=1) the angle of diffraction is small, and the linear dispersion is constant.

Applying the above result, one pixel corresponds to

$$p = \frac{\lambda_2 - \lambda_1}{X_2 - X_1}, \tag{4.9}$$

where p is number of wavelength in units of λ per pixel. The wavelength range then starts at

$$\lambda_{start} = \lambda_1 - p * X_1. \tag{4.10}$$

The entire wavelength range for one image is then given by

$$\lambda_n = \lambda_{start} + k * p, \tag{4.11}$$

where k is the pixel number ranging from 0 - 239 (image dimension in direction of wavelength) in each window. With the wavelength calibration a digitizer resolution of approximately 5 Å per pixel was found.

4.1.7 Absolute (Intensity) Calibration

As mentioned above, this combines two calibrations, an absolute calibration, and a vignetting calibration in the wavelength direction. The calibration is very similar in method to the one described under **Calibration for Vignetting effects**. Instead of normalizing to the median value we must normalize to the actual intensity value. This value is determined by the standard lamp used for calibration. The emission for the used standard lamp (see figure 4.7) is a black body radiation and is described by

$$I = \left[4.79 \cdot 10^{17} \cdot \lambda^4 \left(\exp\frac{hc}{\lambda kT} - 1\right)\right]^{-1}, \tag{4.12}$$

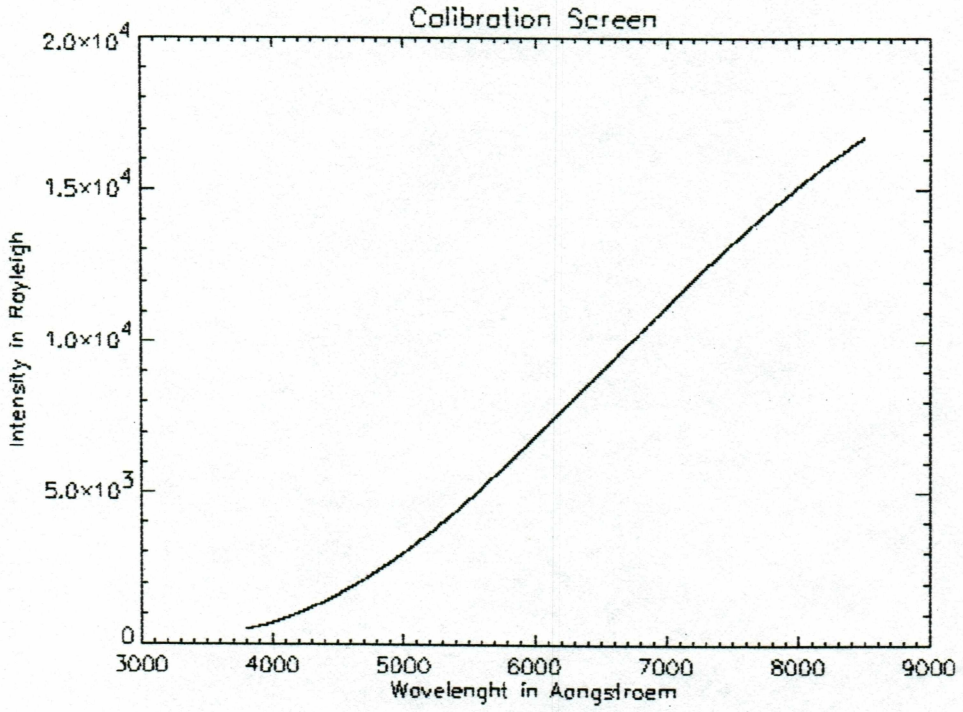

Figure 4.7. The emission curve from the standard lamp measured in Rayleigh as function of wavelength in Ångstrom.

where $4.79 \cdot 10^{17}$ is a constant determined from the standard lamp, λ is the wavelength in meter, $h = 6.63 \cdot 10^{-34}$ Js is Planks constant, $c = 3 \cdot 10^8$ m/s is the speed of light, $k = 1.38 \cdot 10^{-23}$ J/K is Boltzmann's constant, and $T = 3094$ K is the temperature[3].

The vignetting correction in the slit direction was done by normalizing to an average value representing the intensity near the center of each column in the image. In the wavelength direction we need to normalize to the intensity of the standard lamp. Five standard lamp images are normalized to standard lamp intensity. Two averaging procedures are involved here. First we average over the 5 images (pixel by pixel). Then we average over several rows of the image to smoothen out the signal. The next step is to normalize to the known spectral response of the standard lamp. Finally inverting it gives us the calibration image to multiply the data image with. Let X_a be the total averaged image. Then the calibration image is

$$X_{cal} = I * X_a^{-1} \tag{4.13}$$

[3]The constants used here can be found in the log book for the standard lamp located at the Geophysical Institute, Fairbanks, Alaska.

Table 4.1. The transmission coefficient for the first negative (0,1), first positive (3,1), and Meinel (2,0).

Emission	wavelength (Å)	Transmission coefficient (%)
1N (0,1)	3914	94.1
1P (3,1)	7627	98.8
M (2,0)	7852	99.0

4.1.8 Atmospheric Corrections

A ground-based observation of the aurora yields the brightness of the aurora. However, the brightness is not the true emission from the aurora. The atmosphere absorbs and scatters the emission between the source region and ground. The effects are Rayleigh Scattering, absorption by Ozone and water wapor, and ground reflection (ground albedo). *Stamnes and Witt* [1987] calculated transmission coefficients for 310 nm, 350 nm, 555 nm, and 630 nm for different ground albedos. Interpolating between the values and extrapolating to 790 nm, we come up with transmission coefficients for the first negative (0,1) emission, the first positive (3,1) emission and the Meinel (2,0) emission. Table 4.1 gives the transmission coefficients for the 3 emissions. Thus, the observed brightness is e.g. 94.1 % of the 1N(0,1) emission.

4.2 Data Analysis

Of the 5 wavelength regions provided by the instrument, only two are of interest here (4200 and 7700 Å). The data show a vignetting effect towards the edges, and the intensifier's sensitivity in the far blue region is poor. For these reasons the 2 emissions of interest have been chosen to be the first negative $(0,1)$ at 4278 Å and the Meinel $(2,0)$ at 7852 Å. These two bands are both located near the center of the respective windows. Thus any errors due to the vignetting effect and decreasing sensitivity of the intensifier are small. Figure 4.8 shows two typical spectra from the 4200 Å and 7700 Å windows of the spectrograph.

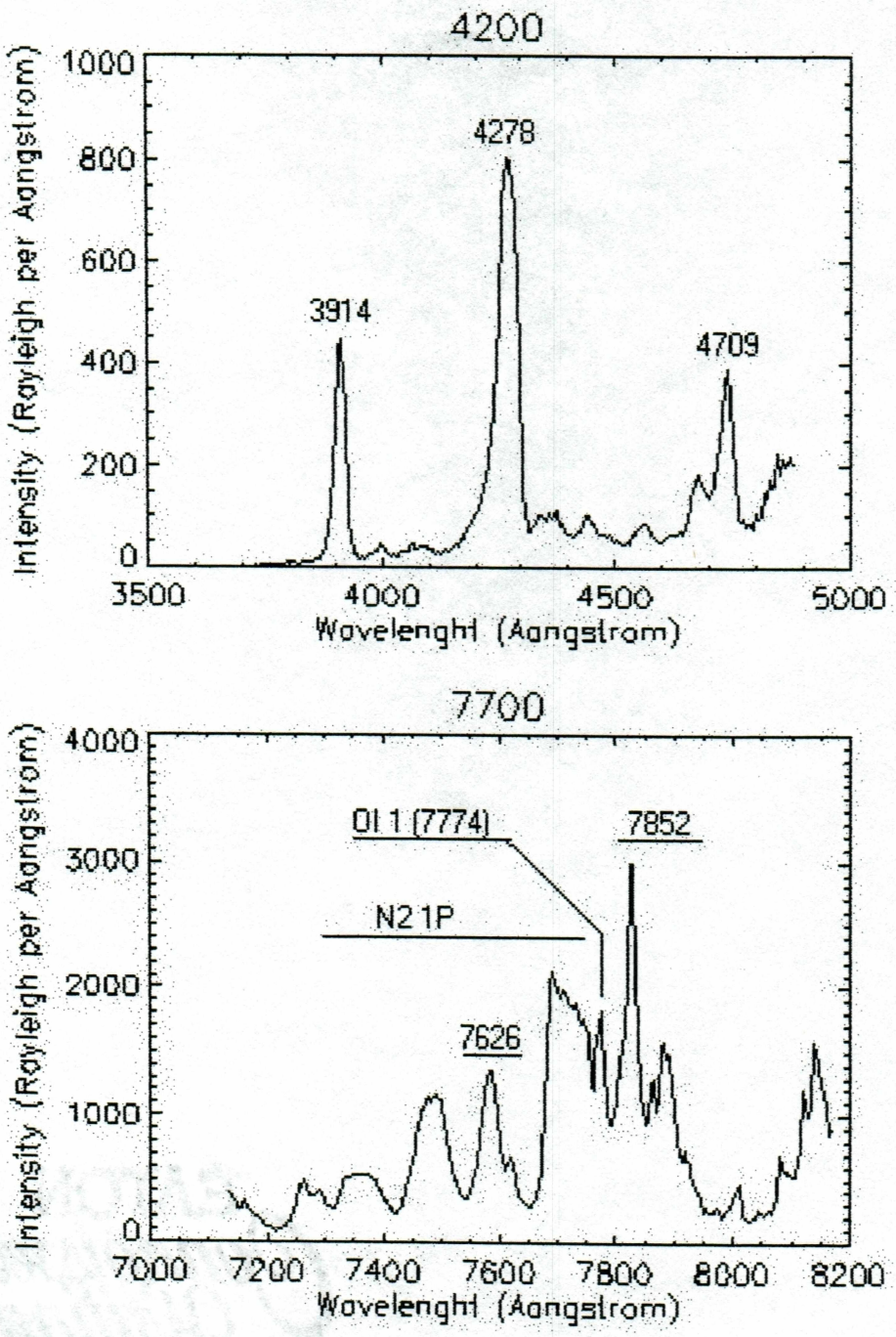

Figure 4.8. A typical spectra from the 4200 and 7700 ranges showing the brightness as a function of wavelength. These spectra was obtained during relative strong auroral activity. The emissions relative close to the 4278 and 7852 emissions are also identified.

4.2.1 Calculating the Emission

In order to compare the emission between the two bands we need the *total* emission, not just the peak of the emission. The total emission is found by integrating over the wavelength spanned by the emissions of interest by using the *trapezoid rule* between two chosen wavelengths. Let the integration be carried out over the two wavelength λ_i, and λ_{i+1}, then the applied algorithm is

$$I = \frac{1}{2}\sum[f(\lambda_i) + f(\lambda_{i-1})] \times (\lambda_i - \lambda_{i-1}), \tag{4.14}$$

where f is the brightness per wavelength.

From the spectra of *Vallance Jones* [1974], the first negative (0,1) at 4278 Å emission is not contaminated by other emissions. However, the line width of the 4278 emission is broader than the separation of the 4278 Å and the first negative emission (1,2) at 4236 Å and we cannot distinguish the two emissions. Thus, the integrated emission contains both emissions. According to *Vallance Jones* [1974], the ratio between the 4278 and 4236 emissions is 7.75 (assuming IBC3 aurora and only electron impact as a source of excitation). The contribution from 4236 is subtracted from the total emission to give the 4278 emission. The Meinel (2,0) at 7852 Å overlaps with the N_2 first positive (7,6) band at 7897 Å. We can find the contribution from this emission if we know the intensity of another emission from the first positive system. The spectra in *Vallance Jones* [1974] shows that the first positive (3,1) emission at 7627 Å can be used for this purpose. The ratio between the (7,6) and (3,1) first positive emissions is 0.05 [*Vallance Jones*, 1974]. The true intensity of the Meinel (2,0) emissions is then the integrated intensity subtracted by the contribution from the first positive (7,6).

Two questions about the Meinel (2,0) and first negative (0,1) are of concern here. First, is the ratio constant or changing? Secondly, if the ratio is constant, what is its value?

If the ratio is constant, there should be a good correlation between the two emissions. To test the correlation a linear Pearson correlation is applied. The Pearson's correlation coefficient is given by

$$r = \frac{\sum_i (x_i - \overline{x})(y_i - \overline{y})}{\sqrt{\sum_i (x_i - \overline{x})^2}\sqrt{\sum_i (y_i - \overline{y})^2}}, \tag{4.15}$$

where x, y are the two emissions, $\overline{x}$ is the mean in the x_i, $\overline{y}$ is the mean in the y_i, and the

summation is over number of data points. A correlation coefficient of +1 indicates a perfect linear relationship, a coefficient of -1 indicates a perfect negative linear relationship, and finally a coefficients of 0 means there is no linear relationship between the two emissions.

In case of a linear relation between the two emissions, a value for the constant ratio can be estimated. To do this a straight line, $y = Ax + B$, is fitted to a scatter plot of the Meinel (2,0) vs. first negative (0,1). The A coefficient is then an estimate for the ratio between the two emissions. A line $y = Ax$ might seems more natural for a fit. But additional emission due to nightglow and sky background might be present in our data, and forcing a $y = Ax$ fit might introduce an error estimate for the ratio. Thus, the B coefficient, if not zero, can be an indication of additional emission due to e.g. nightglow.

To estimate the coefficients A and B, a weighted linear least squares fit is used. Our data are subject to error in both the Meinel (y), and first negative (x) emissions. In addition, the error is not the same for each measurement and thus, each data point y_i, x_i has a standard deviation σ_{xi}, σ_{yi}, respectively. The χ^2 merit function is then

$$\chi^2 = \sum_i \frac{(y_i - B - Ax_i)^2}{\sigma_{yi}^2 + A^2\sigma_{xi}^2} \tag{4.16}$$

The coefficients A and B can be found by minimizing the merit function with respect to A and B. Introducing the weight

$$w_i = \frac{1}{\sigma_{yi}^2 + A^2\sigma_{xi}^2} \tag{4.17}$$

the solution for B is

$$B = \frac{\sum_i w_i(y_i - Ax_i)}{\sum_i w_i} \tag{4.18}$$

Unfortunately the solution for A is non-linear. To find the zero of this non-linear function *Brent's method* is used [*Press et al.*, 1992]. Eq. 4.18 is used in each step solving for A to ensure that the minimum is a minimum with respect to both A and B. To find the error estimates for A and B, σ_A and σ_B the procedure outlined in *Press et al.* [1992] is used.

4.2.2 Error Analysis

Going from the original image to obtaining a value for the emission several procedures have been applied. Each of them introduce an error which will propagate throughout the analysis

and influence the final result. In order to give our estimated values any significance we must include an estimate for the errors as well.

The operations performed on the raw image can be divided into two parts. The first involves pixel to pixel operations and the last involves averaging over pixels.

The pixel to pixel operations involved is the subtraction of noise (dark current + read-out noise) and making a uniform image (flatfield). If we let our raw signal be N, the noise B, and flatfield correction is F, then our signal S^* is

$$S^* = (N - B) \cdot F \tag{4.19}$$

For the absolute calibration (intensity calibration) we averaged over several rows and ended up with a one-row signal representing the part of the image we are interested in. The final image, S, can be written as

$$S = S^* \cdot A, \tag{4.20}$$

where A is the factor for the absolute calibration.

To obtain intensity values the trapezoid rule was applied

$$I = \frac{1}{2} \sum [S(\lambda_i) + S(\lambda_{i-1})] \times (\lambda_i - \lambda_{i-1}). \tag{4.21}$$

The error is calculated by letting S be a function N, B, F, and A. Then the error in S is

$$\delta S = \sqrt{\left(\frac{\partial S}{\partial N}\delta N\right)^2 + \left(\frac{\partial S}{\partial B}\delta B\right)^2 + \left(\frac{\partial S}{\partial F}\delta F\right)^2 + \left(\frac{\partial S}{\partial A}\delta A\right)^2} \tag{4.22}$$

Both N and B are obtained from a counting device (the CCD camera) and the error in them are then $\sqrt{N}$ and $\sqrt{B}$, respectively. The error in F and A involves both averaging and addition arithmetic. Where averaging is applied, the error in the mean σ_m is calculated

$$\sigma_m = \frac{\sqrt{\frac{\sum_i (x_i - \bar{x})^2}{n-1}}}{n}, \tag{4.23}$$

where x is the measurements to be averaged, $\bar{x}$ is the mean of x, and n is the total number of samples. For addition, a simple rule of addition errors are used

$$\delta x = \delta x_1 + \ldots + \delta x_n. \tag{4.24}$$

For the data set presented here, at typical error of 15% to 20% for the emission values is found.

Chapter 5

Results and Discussion

5.1 Observations

Observations were carried out at Poker Flat Research Range (PFRR) located 30 miles north-east of Fairbanks, Alaska. The imaging spectrograph was orientated towards magnetic zenith, and thus recorded data along the magnetic field lines.

The data presented here have been chosen based on the following :

- Data is not saturated.
- A non-moving aurora during the period of integration.
- A constant emission rate during the period of integration.

Of the recorded data, March 19, 2001, March 23, 2001, and March 31, 2001, had periods of time satisfying the above criteria. The data used to calculate the ratio between the two emissions have in addition been picked based on paired data points. That is, only data points that are recorded successively (a 4200 recording followed by a 7700 recording or vice versa) have been used. In this way a time interval between the 4200 and 7700 recording is approximately 1 - 1 1/2 minute. Figure 5.1 - figure 5.3 shows the time series of the Meinel (2,0) and the first negative (0,1) emissions, and the corresponding time series of the ratio between the two emissions. In order to better determine the activity observed in the data obtained with the imaging spectrograph, all-sky data from Poker Flat are available for the two nights of March 19 and March 23. Meridian Scanning Photometer (MSP) data are

available for all three nights. The correlation and error given for the three nights in the following section are the result of the error analysis described in the previous chapter.

March 19 : The overall activity as seen in the data from the imaging spectrograph seems correlated for the two emissions. However, there are times, where the activity does not seem to follow each other. Around 6:20 UT the first negative emission is decreasing while the Meinel is increasing. In addition, the first negative emission is close to the same order of magnitude as the Meinel emission. No explanation has been found for this so far. The Meinel maximum at 7:17 UT is not seen in the first negative. However, the following sequence of the first negative shows a decay in the emission, which is also the case for the Meinel emission. Thus, the missing maximum in the first negative can be a result of non-simultaneous data, that is, no data are available for the first negative at the same time. A peak in the Meinel at 7:30 UT is apparently associated with a small dip in the first negative emission. This feature is left unexplained. From 7:39 UT the first negative emission is increasing, while the Meinel increases to a maximum and then decreases. Again, this feature leaves no explanation. Near 8:50 UT a couple of data points were recorded. As little as can be said about two data points, they do show the same characteristics. The observed minimum in the first negative at 9:37 UT is associated with increased Meinel activity. The first negative activity right before and after shows a nearly constant emission of 50 kR. At this point, no explanation for this minimum is made. At last, the Meinel decays, while the first negative has a small increment. No further data is observed for this night.

The all-sky camera (see figure 5.4) can tell more about the detailed structure of the aurora than the data set presented here. From 6:00 UT to 8:00 UT a diffuse aurora with some intensity variations were present. In the interval from 8:00 UT to 9:15 UT not much activity is observed with the all-sky camera. 9:20 UT to 10:15 UT shows a period with high activity with an poleward moving arc as the dominant feature. Intensity variations within the active regions are also observed. The time interval between measurements in the imaging spectrograph ranges from 1 minute to 1 1/2 minute. Thus, if the intensity variations shown in the all-sky data are of the order of seconds or tens of seconds, they will not show up in the imaging spectrograph.

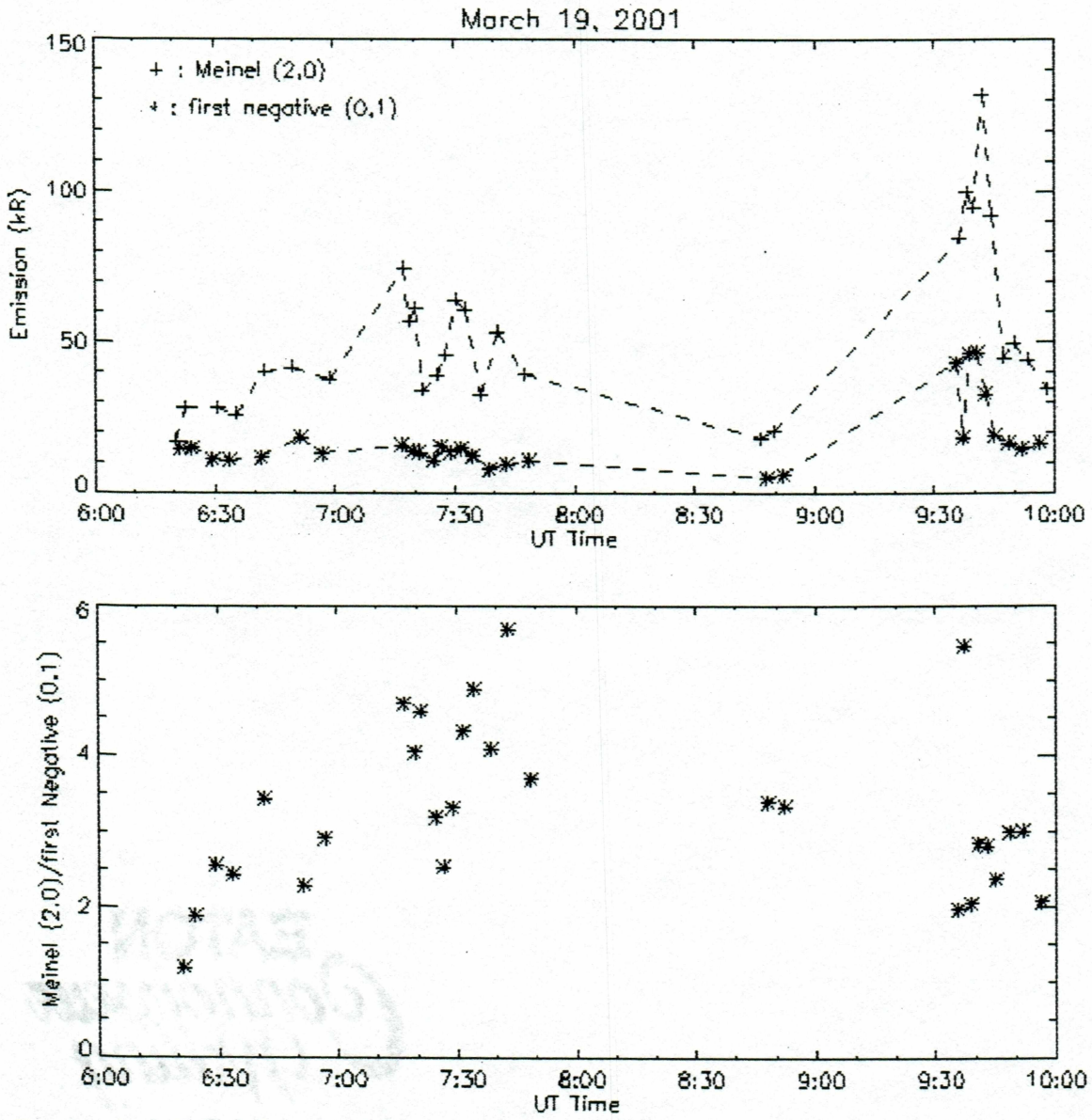

Figure 5.1. First plot showing the time series of Meinel (2,0) and first negative (0,1) emissions, March 19, 2001. Second plot shows the corresponding time series of the Meinel (2,0) and first negative (0,1) ratio.

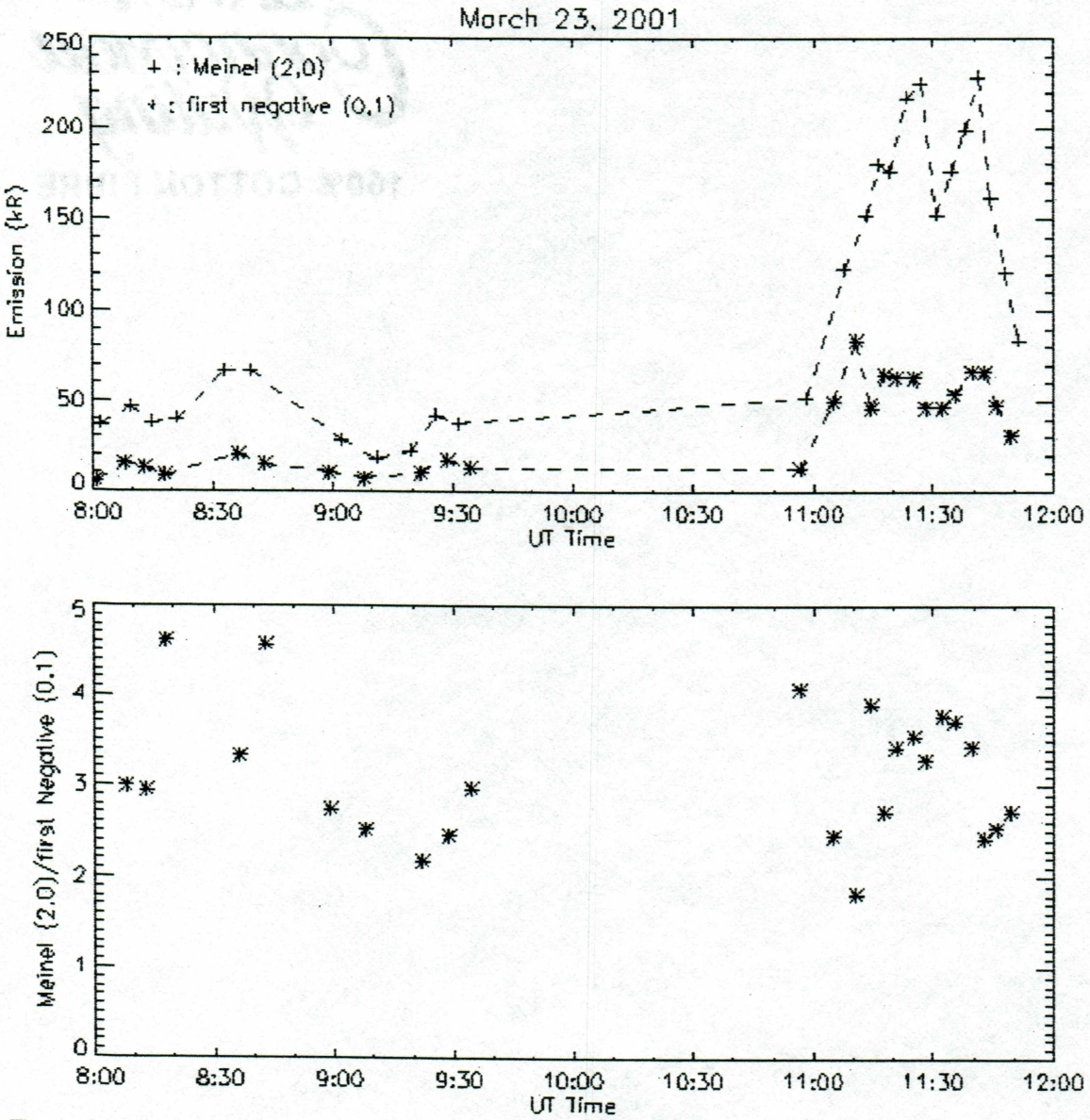

Figure 5.2. First plot showing the time series of Meinel (2,0) and first negative (0,1) emissions, March 23, 2001. Second plot shows the corresponding time series of the Meinel (2,0) and first negative (0,1) ratio.

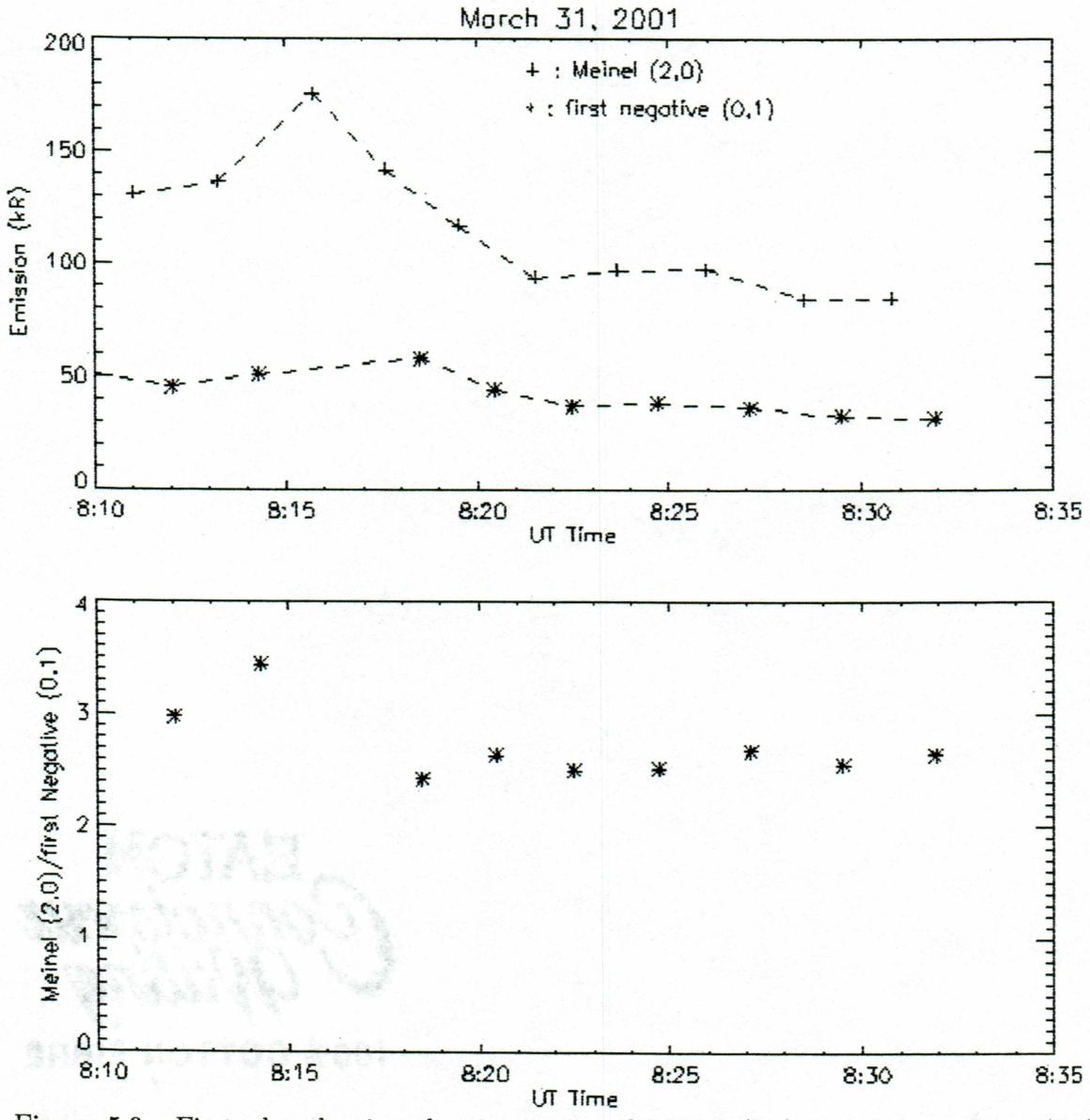

Figure 5.3. First plot showing the time series of Meinel (2,0) and first negative (0,1) emissions, March 31, 2001. Second plot shows the corresponding time series of the Meinel (2,0) and first negative (0,1) ratio.

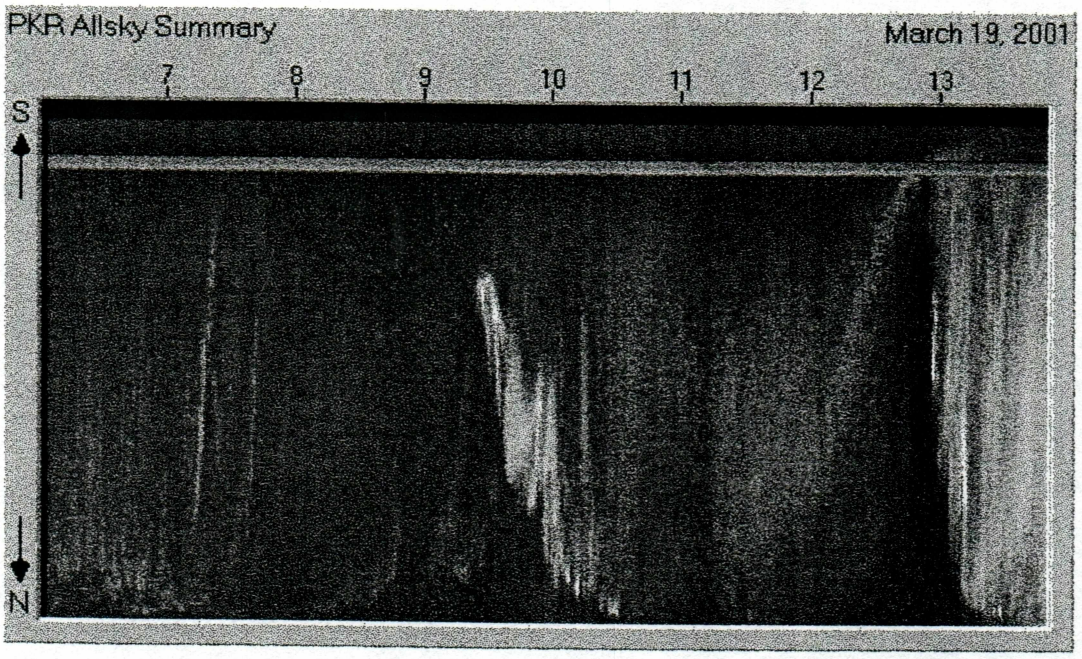

Figure 5.4. Time series for auroral activity seen with the All-sky camera located at Poker Flat, March 19, 2001. The time scale shown is in UT time while the spatial scale ranges from north to south.

Thus, the discrepancies discussed above are likely to be due to short time intensity variations in the aurora.

The ratio shows scatter between values of 1-6 during the period of observation. The period from 9:15 UT to 10:00 UT which is associated with high auroral activity shows a consistent collection of values between 2-3 expect from a single point at 5.5. This single point is associated with the minimum in the first negative described earlier. The scatter plot in figure 5.5 shows the linear fit and estimate a value of 2.53 ± 0.38 for the emission ratio. The correlation coefficient is 0.80.

March 23 : The night of March 23 shows a very good correlation between the two emissions for both low activity (8:00 UT to 9:30 UT), and high activity (11:00 UT to 12:00 UT). Both periods show a diffuse aurora with very few intensity variation, and thus, are well suited for a measurement of the ratio between the two emissions under different activity conditions. The only two times where the correlation seems to fail is

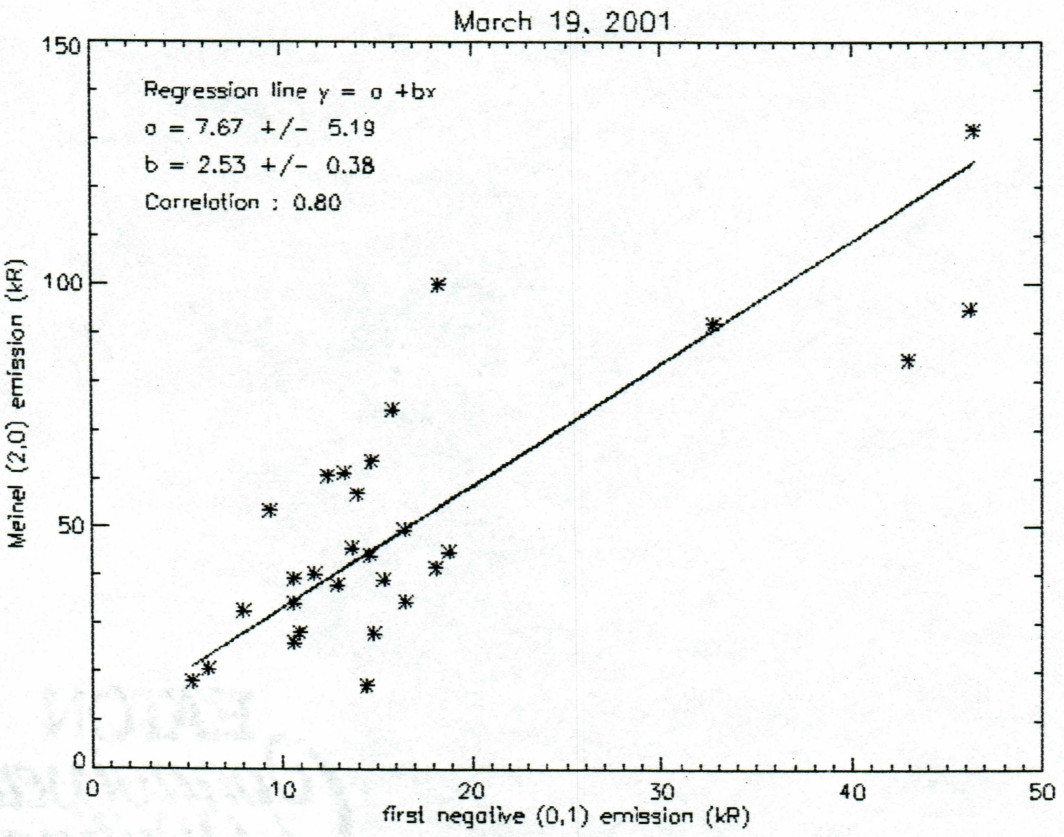

Figure 5.5. Scatter plot of the Meinel (2,0) and first negative (0,1), March 19, 2001. A linear regression line is superimposed upon the plot and the regression parameters shown. In addition, the correlation coefficient is given.

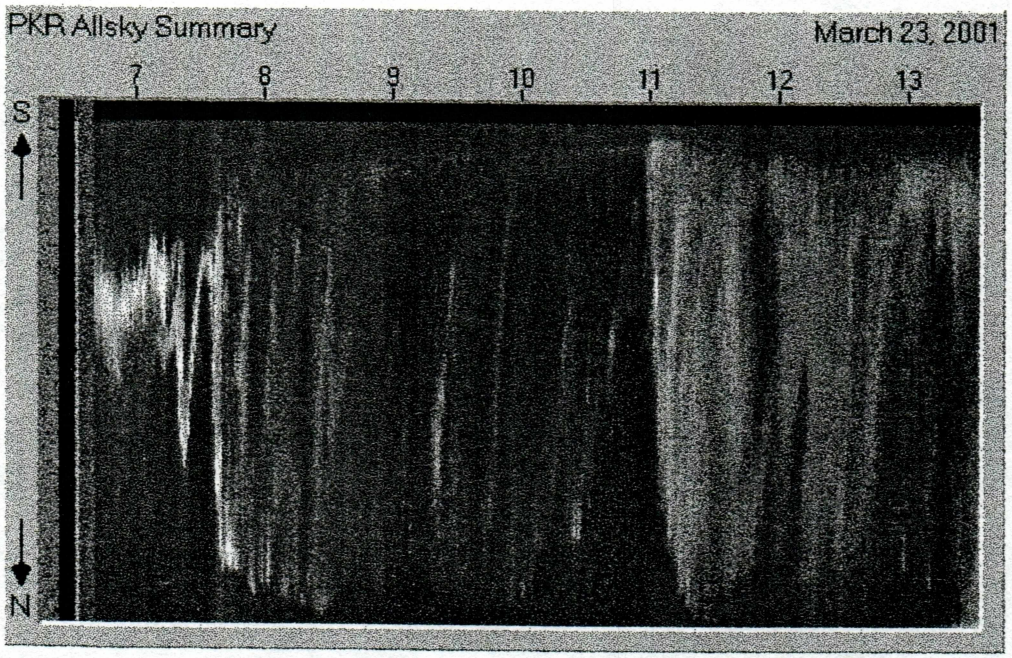

Figure 5.6. Time series for auroral activity seen with the All-sky camera located at Poker Flat, March 23, 2001. The time scale shown is in UT time while the spatial scale ranges from north to south.

near 11:15 UT where a dip is observed in the first negative emission, but not present in the Meinel observation. From the all-sky data (figure 5.6), we can see, that near that time there is a variation in the intensity. The observed different pattern might be due to rapid fluctuations in the intensity. The second occasion occurs at 11:20 UT, where the first negative shows a small decrease but otherwise remains constant. A decay is also seen weakly in the Meinel before an increment to about 230 kR. Only two observations are made at this peak, and both fall between the first negative observation at 11:20 UT and the next first negative observation. Thus, a simultaneous observation of the first negative in that interval might have shown an increase in the first negative as well. Again, the period of time where the correlation is weak, might be due to non-simultaneous observations.

The values of the ratio obtained this night show more consistency than the previous night. Values ranges here between 2 and 5. There is no evidence for a pattern related to the auroral activity throughout the data set. The scatter plot (figure 5.7) shows a

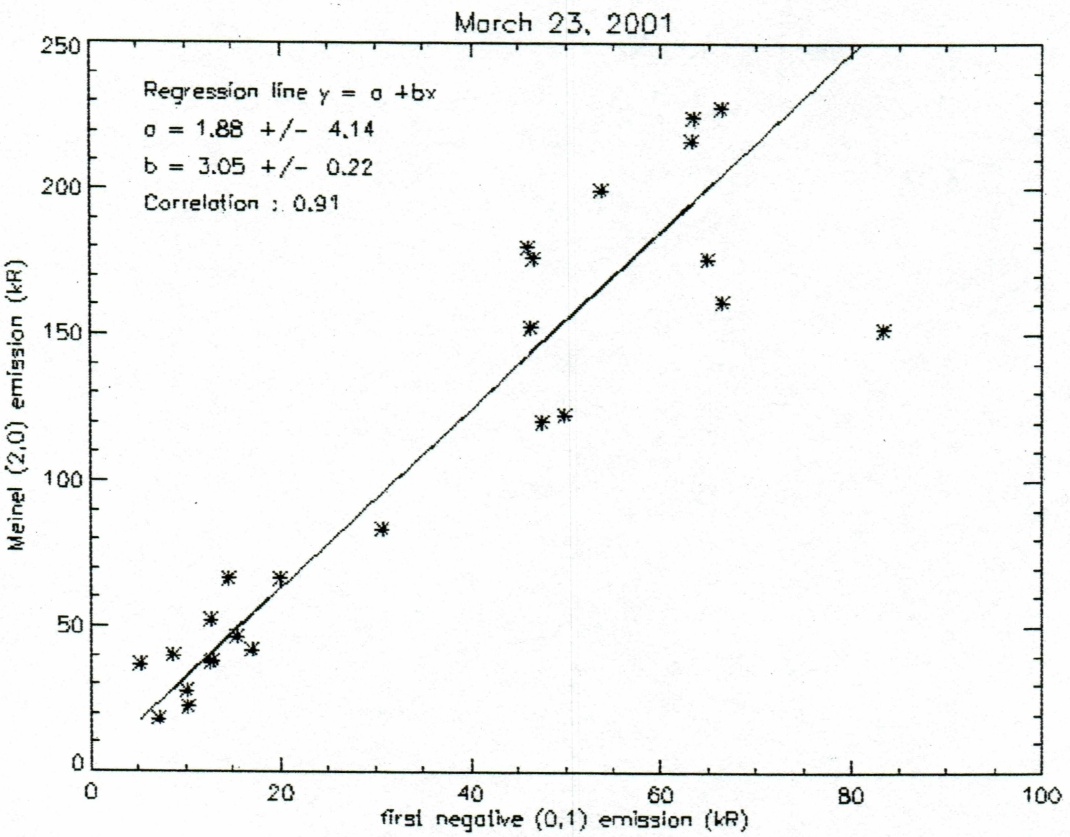

Figure 5.7. Scatter plot of the Meinel (2,0) and first negative (0,1), March 23, 2001. A linear regression line is superimposed upon the plot and the regression parameters shown. In addition, the correlation coefficient is given.

very close fit to a straight line with a correlation coefficient of 0.91. The data point at high first negative energy deviates most from the fit. At the time for this observation, the intensity increased and the poor fit might be due to the fact that the time between two recordings is too long compared to the time scale of which the aurora changes at this point. An estimated value for the ratio is found to be 3.05 ± 0.22.

March 31 : No all-sky data were available March 31. However, MSP data show a strong diffuse aurora from 8:10 UT to 8:35 UT during the time of observation with the imaging spectrograph. Apparently the two emission curves follows each other well.

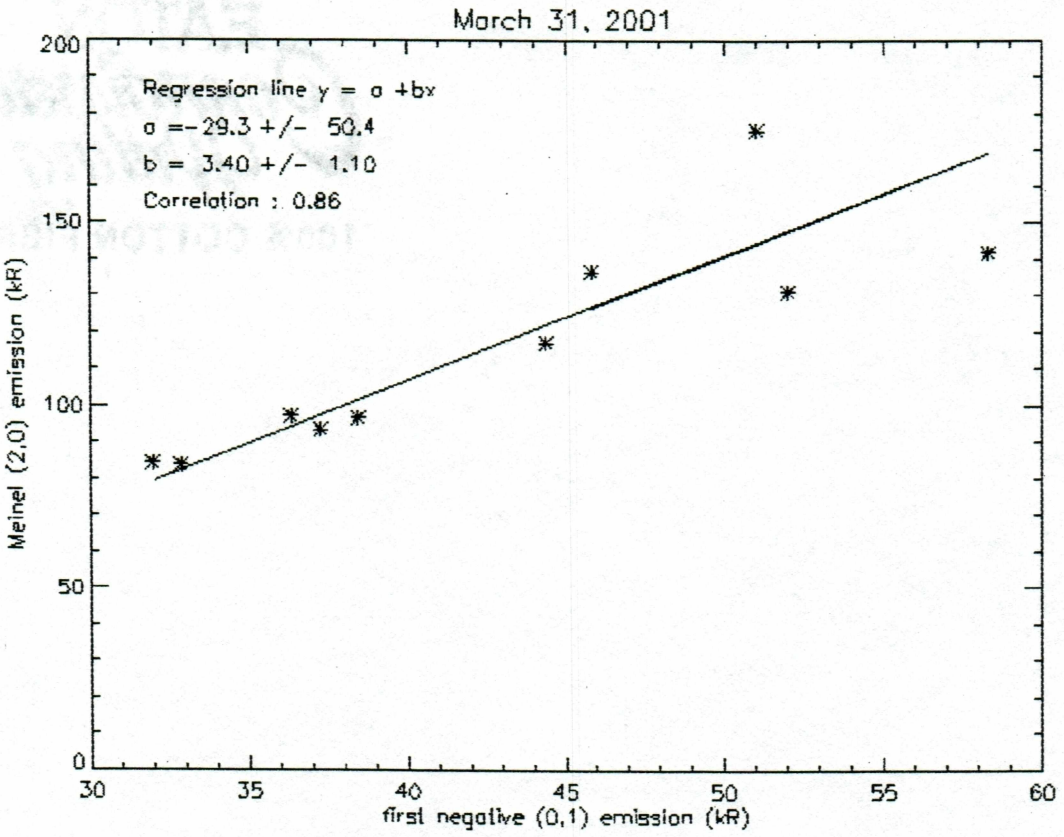

Figure 5.8. Scatter plot of the Meinel (2,0) and first negative (0,1), March 19, 2001. A linear regression line is superimposed upon the plot and the regression parameters shown. In addition, the correlation coefficient is given.

The peak occurring near 8:16 UT in the Meinel band is not seen simultaneously in the first negative. But there should be no doubt from the neighboring data points of the first negative, that a peak might have been observed if simultaneous data had existed.

The ratios is fairly constant within the period of observation. The data set fits very well to the linear fit (see figure 5.8) with an estimated ratio of 3.40 ± 1.10 . The correlation coefficient for this plot is estimated to be 0.86.

5.2 Discussion

The ratio between the Meinel (2,0) and first negative (0,1) obtained in this analysis vary between 1-6 with most scatter seen in the observations of March 19. All three nights presented here show good correlation with correlation coefficients of 0.80, 0.91, and 0.86, respectively. The scatter plots have been fitted to a straight line by linear regression and the proportionality constant between Meinel (2,0) and first negative (0,1) have been determined. During three nights of observations, ratios of 2.53 ± 0.38, 3.05 ± 0.22, and 3.40 ± 1.10 were found.

Remick et al. [2001] observed a decrease in the ratio during moderate active aurora, and attributed that to an increase in the first negative emission. The ratio presented by *Remick et al.* [2001] shows variation of up to a factor of 10. Such large variation is not observed here. The ratio remains fairly constant regardless of auroral activity. An important note about the previous results should be mentioned. *Remick et al.* [2001] collected spectra at 3 minute intervals, and thus variations in the aurora with a time scale less than 3 minutes cannot be determined. A strong aurora will likely have variation less than 3 minutes, even less than 1 minute which is the absolute best estimate between two successive recordings of the Meinel (2,0) and first negative (0,1) that can be done by the imaging spectrograph used in this analysis.

The values estimated for the ratio have to be compared to the values of 2.18 [*Vallance Jones*, 1974], 2.5 [*Henriksen*, 1984], and 2.2 using the transition probabilities given by *Lofthus and Krupenie* [1977]. The value of 2.2 is obtained assuming only electron impact are present. *Henriksen* [1984] observed the two emissions simultaneously during low auroral activity (IBC1), while the value of 2.18 from *Vallance Jones* [1974] is based on an IBC3 aurora. The value of 2.18 is within the experimental error of the night of March 19, while the result by *Henriksen* [1984] is within the experimental error of both March 19 and March 31.

There are three possibilities for this higher ratio. Either there is an increase in the Meinel (2,0) emission or the first negative (0,1) emission is decreased and last, the values for the emissions are affected by the calibration.

Some mechanism which can change the population of the N_2^+ A and B states beside

electron impact, have been discussed earlier in this thesis. Two of the mechanisms are quenching of the A state and photon excitation of the ion ground state into the B state. The aurorae observed here are relative strong and penetrate deeper into the atmosphere. Quenching of the A state would decrease the Meinel emission instead of increasing it. Thus quenching cannot describe the higher ratio observed here. Also, quenching is dependent on auroral activity and we would expect a changing ratio. This is not observed either. The first negative emission can be enhanced by resonance scattering. This requires N_2^+ molecules being transported into sunlit regions. Such an up-welling of N_2^+ has been observed [*Romick et al.*, 1999], and showed a dependence on auroral activity, with a higher intensity observed at high aurora activity. This would imply a changing ratio as a function of activity, and would also decrease the ratio predicted. Neither of these effects are observed in this experiment and we conclude that an upwelling of N_2^+ does not occur during the periods observed here.

The possibility that the ratio between the excitation cross sections for proton/hydrogen impact is sensitive to impact energy was also left as an option to explain a changing ratio. The H_β emission have been identified in the auroral spectra obtained with the imaging spectrograph. Of the three nights only March 19 showed a variation in H_β emission. If proton excitation would favor either of the two states, we would expect to observe a variation in the ratio similar to the variation in H_β. Such a variation was not observed during the night of March 19, and we exclude the possibility that proton excitation favors the A or B. One comment should be mentioned here. The meridian scanning photometer (MSP) located at Poker Flat, Alaska, observed no emission associated with the H_β emission. However, the signature of the H_β emission is clear in the spectra from the imaging spectrograph. Why this is not seen in the MSP could be related to instrumental problems with the MSP[1]

Our estimate for the Meinel (2,0) might be too high due to additional emission from sky background and nightglow. The red part of the visible spectrum is more easily excited compared to the blue part of the spectrum. As seen in the scatter plots for the three nights, the A coefficient (the intercept of the intensity axis) is positive. This shows that additional emission besides aurora are present. If this contribution is removed the obtained ratio is

[1]Private communication, H. C. Stenbaek-Nielsen and D. Lummerzheim, Geophysical Institute, Fairbanks, Alaska.

in even better agreement with the published values from [*Vallance Jones*, 1974; *Henriksen*, 1984; *Lofthus and Krupenie*, 1977]. Finally, the data presented here are obtained during moderate strong to strong aurora (K_p 4 to 9). Under these conditions we can expect low-energetic electrons as well. Low-energetic electron impact upon the ion will increase the A state relative to the B state and thus, we will expect a higher ratio between the two emissions. The night of March 31 is recorded during a K_p 9 aurora. During such strong aurora we expect more soft-electron precipitation and emissions in the red. This is confirmed by a larger ratio than the two previous nights.

However, we must still consider one other possibility, that the values estimated here are too high due to errors introduced in the calibration . Thus, we must ask ourself if we can trust the values obtained with the instrument.

The emission values presented here seem very high. However, they are obtained during strong to very strong auroral activity. Is the calibration estimating the values too high? One way to check this is to go through the entire calibration process with an image obtained from the standard lamp and compare it to the values of the known emission of the standard lamp. If the values agree we must conclude that the calibration process is good. Using standard lamp images from the 4200 and 7700 window, we find they are in good agreement with the given values. Thus the calibration seems to be in order. But there are indications that contradict this. First, the ratio between the 3914 and 4278 emissions should be of the order of 3 [*Vallance Jones*, 1974], that is, the 3914 emission should be 3 times brighter than the 4278 emission. As seen in the spectra figure 4.8 this is not even close. It looks more like the 4278 are two times *brighter* than 3914. Also, the ratio between the 4278 and 4709 emission should be close to 5 [*Vallance Jones*, 1974], but the value found here is a little less than 3. The 4709 emission is present in both the 4200 and 4800 window. Investigating two consecutive measurements in the two windows yields different result for the integrated intensity of the 4709 emission. However, the two values are within the determined error of each other. Also, the difference between the two values are not consistent but differ from less than 1 % to 20 % . The inconsistency of the difference can be explained by changes in the aurora between the two recordings. If the difference was due to the calibration we would expect a consistent difference. Finally, the result of the integrated intensity seems to be very sensitive to the intensity calibration. The results presented here are averaged

over several rows of the image near the center, representing a region of the CCD covering magnetic zenith. If we instead are using just the center row for the result we obtain a ratio *less* than previous published values. Thus, by choosing a slightly different approach we can obtain values less or greater than previous found results. At this point no explanation is found to explain the contradictions described above.

Chapter 6

Conclusion

The intensity of the first negative (0,1) emission at 4278 Å and Meinel (2,0) at 7852 Å have been recorded for three nights, and the ratio between the two have been analyzed. The experiment has a time resolution of approximately 100 seconds depending on the auroral activity. However, as seen in the data set, changes in auroral activity can occur on a much smaller time scale.

The results presented in this thesis showed a constant ratio regardless of auroral activity. The ratio obtained is 2.53 ± 0.38, 3.05 ± 0.22, and 3.40 ± 1.10 for the three nights of observations. This value is higher than previous suggested. The constant ratio independent of activity rules out the previous discussed mechanism that could cause a changing ratio. Quenching of the $N_2^+(A)$ state being one of them. Quenching would change the Meinel emission as a function of activity and thus change the ratio. Also, an up-welling of N_2^+ into sunlit regions would increase the first negative emission due to resonant scattering. This process is also dependent on auroral activity and would cause a changing ratio as well. The proposed charge transfer process de-activates the $N_2^+(A)$ state. However, the transition observed in this experiment is not influenced by the charge transfer process, and no effect should be detected. Unless the quenching factor or the resonance scatter is constant for the different activity levels observed here, both processes have to be excluded. The ratio of proton/hydrogen excitation cross sections for the A and B states is shown not to be sensitive to impact energy.

The difference in the observed value compared to the previous published values [*Vallance Jones*, 1974; *Henriksen*, 1984; *Lofthus and Krupenie*, 1977] are concluded to be due

to either limitation in the instruments ability to record simultaneous data of the Meinel (2,0) and first negative (0,1), additional emission from nightglow present in the data, soft-electron precipitation into the upper atmosphere, or errors introduced in the calibration of the instrument. In order to determine the influence the above processes have on the ratio and its value, simultaneous recording have to be performed and sky background be subtracted. There are indications of errors in the calibration. The ratio between the 3914 and 4278 emissions are off by as much as a factor of 6 while the ratio between 4278 and 4709 is found to be 3-4 when it should be close to 5. So far no explanation can be given to these discrepancies.

Bibliography

Ajello, J. M., Emission Cross Sections of N_2 in the Vacuum Ultraviolet by Electron Impact, *J. Chem. Phys.*, *53*, 1156 , 1970.

Borst, W. L., and E. C. Zipf, Cross section for electron-impact excitation of the (0, 0) first negative band of N_2^+ from threshold to 3 keV, *Phys. Rev. A*, *1*, 834, 1970.

Brekke, A., and A. Egeland, *The Northern Lights, their heritage and science*, Grøndahl Dreye, 1994.

Broadfoot, A. L., Resonance scattering by N_2^+, *Planet. Space Sci.*, *15*, 1801 , 1967.

Cartwright, D., W. R. Pendleton Jr., and L. D. Weaver, Auroral Emission of the N_2^+ Meinel Bands, *J. Geophys. Res.*, *80*, 651 , 1975.

Christensen, L. L., A. V. Olesen, and M. van der Poel, *Lysfænomer i naturen*, Høst & Søn, 1998.

Degen, V., Vibrational enhancement and the excitation of the N_2^+ and the first negative system in the high-altitude red aurora and the dayside cusp, *J. Geophys. Res.*, *86*, 11,372 , 1981.

Doering, J. P., and L. Goembel, Direct experimental measurement of electron impact ionization-excitation branching ratios. 1. Results for N_2 at 100 eV, *J. Geophys. Res.*, *96*, 16025, 1991.

Doering, J. P., and J. Yang, Comparison of the electron impact cross section for the N_2^+

first negative (0,0) band at 3914 Å measured by optical fluorescence, coincidence electron impact, and photoionization experiments, *J. Geophys. Res.*, *101*, 19723, 1996.

Doering, J. P., and J. Yang, Direct experimental measurement of electron impact ionization-excitation branching ratios. 3. Branching ratios and cross sections for the N_2^+ $X^2\Sigma_2^+$, $A^2\Pi_u$, and $B^2\Sigma_u^+$ states at 100 eV, *J. Geophys. Res.*, *102*, 9683, 1997.

Espy, P. J., W. R. Pendleton Jr., G. G. Sivjee, and M. P. Fetrow, Vibrational development of N_2^+ Meinel band system in the aurora, *J. Geophys. Res.*, *92*, 11,257 , 1987.

Fons, J. T., J. S. Allen, R. S. Schappe, and C. C. Lin, Production of electronically excited N_2^+ ions by electron impact on N_2 molecules, *Phys. Rev. A*, *49*, 927, 1994.

Fox, J. L., and A. Dalgarno, The vibrational distrubition of N_2^+ in the terrestrial ionosphere, *J. Geophys. Res.*, *90*, 7557 , 1985.

Gattinger, R. L., Master's thesis, University of Saskatchewan, Saskatoon, 1961.

Gattinger, R. L., and A. Vallance Jones, The intensity ratios of auroral emission features, *Ann.Geophys.*, *28*, 91 , 1972.

Gattinger, R. L., and A. Vallance Jones, N_2^+ Meinel auroral spectra in the 1.5 μ region, *Can. J. Phys.*, *51*, 287, 1973.

Goembel, L., J. Yang, and J. P. Doering, Direct experimental measurement of electron impact ionization-excitation branching ratios. 2. Angular distribution of secondary electrons from N_2 at 100 eV. , *J. Geophys. Res.*, *99*, 17477, 1994.

Gray, D. F., *The observation and analysis of stellar photospheres*, Cambridge University Press, 1992.

Halas, S., and B. Adamczyk, Cross sections for the production of N_2^+, N^+, and N_2^{++} from nitrogen by electrons in the energy range 16-600 eV, *Int. J. Mass Spectrom. Ion Phys.*, *10*, 157, 1972.

Harrison, A. W., Recent observations of the auroral spectrum between 1.02 μm and 1.13 μm, *Can. J. Phys*, *47*, 599, 1969.

Harrison, A. W., Spectrophotometry of the aurora, *Can. J. Phys*, *50*, 500, 1972.

Henriksen, K., N_2^+ emissions in sunlit cusp and night-side aurora, *Ann. Geophys.*, *2*, 457 , 1984.

Holland, R. F., and W. B. Maier II, Study of the $A \rightarrow X$ transition in N_2^+ and CO^{+*}, *J. Chem. Phys.*, *56*, 5229 , 1972.

Holland, R. F., and W. B. Maier II, Erratum : Study of the $A \rightarrow X$ transition in N_2^+ and CO^{+*}, *J. Chem. Phys.*, *58*, 2672, 1973.

Itakawa, Y., M. Hayashi, A. Ichimura, K. Omda, K. Sakimoto, K. Takayanagi, M. Nakamura, and T. Takayanagi, Cross sections for collisions of electrons and photons with nitrogen molecules, *J. Phys. Chem. Ref. Data*, *15*, 985, 1986.

Lofthus, A., and P. H. Krupenie, The spectrum of molecular nitrogen, *J. Chem. Phys. Ref. Data*, *6*, 113, 1977.

Märk, T. D., Cross section for single and double ionization of N_2 and O_2 molecules by eletron impact from threshold up to 170 eV, *J. Chem. Phys.*, *63*, 3731, 1975.

Oddone, S., J. W. Sheldon, K. A. Hardy, and J. R. Peterson, Dissociative recombination of the $A^2\Pi_u$ and the $X^2\Sigma_g$ states of N_2^+ in a glow discharge, *Phys. Rew. A*, *56*, 4737 , 1997.

Omholt, A., The red and near-infra-red auroral spectrum, *J. Atmos. Terr. Phys.*, *10*, 320 , 1957.

Pendleton Jr., W. R., and L. D. Weaver, Excitation and de-excitation properties of $N_2^+(A^2\Pi_u)$, final technical report, Technical Report Arpa order 1691, contract F 33657-71-C-0174, Advan. Res. Proj. Agency, Washington D. C., 1973.

Piper, L. G., B. D. Green, W. A. M. Blumberg, and S. J. Wolnik, N_2^+ Meinel band quenching, *J. Chem. Phys.*, *82*, 3139 , 1985.

Piper, L. G., B. D. Green, W. A. M. Blumberg, and S. J. Wolnik, Electron impact excitation of the N_2^+ Meinel band, *J. Phys. B: At. Mol. Phys.*, *19*, 3327 , 1986.

Press, W. H., S. A. Teukolsky, W. T. Vetterling, and B. P. Flannery, *Numerical Recipes in C*, Cambridge University Press, 1992.

Rapp, D., and P. Englander-Golden, Total cross sections for ionization and attachment in gasses by electron impact, I, Positive ionization, *J. Chem. Phys.*, *43*, 1464, 1965.

Rees, M. H., On the interaction of auroral protons with the Earth's atmosphere, *Planet. Space Sci.*, *30*, 463 , 1982.

Rees, M. H., *Physics and chemistry of the upper atmosphere*, Cambridge University Press, 1989.

Remick, K., R. W. Smith, and D. Lummerzheim, The significance of resonant scatter in the measurement of N_2^+ first negative 0-1 emission during auroral activity, *J. Atmos. Solar-Terr. Phys.*, *63*, 295, 2001.

Romick, G. J., J.-H. Yee, M. F. Morgan, D. Morrison, L. J. Paxton, and C.-I. Meng, Polar cap optical observations of topside (> 900 km) molecular Nitrogen ions , *Gephys. Res. Lett.*, *26*, 1003 , 1999.

Semeter, J. L., *Ground-based tomography of atmospheric optical emissions*, Ph.D. thesis, Boston University, 1997.

Shemansky, D. E., and A. L. Broadfoot, Excitation of N_2 and N_2^+ systems by electrons, 2, Excitation cross sections and $N_2 1PG$ low pressure afterglow, *J. Quant. Spectrosc. Radiat. Transfer*, *11*, 1401, 1971.

Silverman, S., Early auroral observations, *J. Atmos. Solar-Terr. Phys.*, *60*, 997 , 1998.

Simpson, F. R., and J. W. McConkey, Excitation of the $A^2\Pi u$ state of N_2^+ by electrons, *Planet. Space Sci.*, *17*, 1941 , 1969.

Srivastava, B. N., and I. M. Mirza, Absolute cross sections for simultaneous ionization and excitation o N_2 by electron impact, *Phys. Rev.*, *168*, 86, 1968.

Srivastava, B. N., and I. M. Mirza, Excitation function of the N_2^+ Meinel band by electron impact, *Can. J. Phys.*, *47*, 475, 1969.

Stamnes, K., and G. Witt, The effect of light scattering and diffuse reflection on atmospheric spectral measurements, in *Proc. 13th annual meeting on atmos. studies by optical methods*, Oslo, 1987.

Stanton, P. N., and R. M. S. John, Electron excitation of the first positive bands of N_2 and the first negative and Meinel bands of N_2^+, *J. OPt. Soc. Amer.*, *59*, 252, 1969.

Vaisberg, O. L., Results of researches of the program of the IGY, in *Polar aurora and night airglow*, 8, p. 43, Academy of Sciences of the USSR, Moscow, 1962.

Vallance Jones, A., Auroral spectroscopy, *Space Sci. Rev.*, *11*, 776, 1971.

Vallance Jones, A., *Aurora*, D. Reidel Publ. Co., 1974.

Vallance Jones, A., and R. L. Gattinger, Vibrational development and quenching effects in the $N_2(B^3\Pi_g - A^3\Sigma_u^+)$ and $N_2^+(A^2\Pi_u - X^2\Sigma_g^+)$ systems in aurora, *J. Geophys. Res.*, *83*, 3255 , 1978.

van de Runstraat, C. A., F. J. de Heer, and T. R. Grovers, Excitation and decay of the $C^2\Sigma_u^+$ state of N_2^+ in the case of electron impact on N_2, *Chem. Phys.*, *3*, 431, 1974.

Van Zyl, B., and W. Pendleton Jr., N_2^+ $X^2\Sigma_2^+$, $A^2\Pi_u$, and $B^2\Sigma_u^+$ production in $e^- + N_2$ collisions, *J. Geophys. Res.*, *100*, 23,755, 1995.

Van Zyl, B., and T. M. Stephen, Dissociative ionization of H_2, N_2, and O_2 by electron impact, *Phys. Rev. A*, *50*, 3164, 1994.

Van Zyl, B., M. W. Gealy, and H. Neumann, N_2^+ first negative emission cross sections for low-energy H^+ and H impact on N_2, *Phys. Rev. A*, *28*, 2141 , 1983.

Van Zyl, B., M. W. Gealy, and H. Neumann, Prediction of photon yields for proton aurorae in an N_2 atmosphere, *J. Geophys. Res.*, *89*, 1701 , 1984.

Zipf, E. C., The dissociative recombination of vibrationally excited N_2^+ ions, *Geophys. Res. Lett.*, *7*, 645 , 1980.